Assessment and Uncertainty Quantification of Onshore Geological CO_2 Storage Capacity in China

Ehsan Ranaee[1], Rafi Khattar[1], Fabio Inzoli[1*], Martin J. Blunt[1,2], Alberto Guadagnini[3]

[1]Dipartimento di Energia, Politecnico di Milano, Via Lambruschini 4, 20156 Milano, Italy

[2]Imperial College London, Department of Earth Science and Engineering SW7 2AZ, United Kingdom

[3]Dipartimento di Ingegneria Civile e Ambientale, Politecnico di Milano, Piazza L. Da Vinci 32, 20133 Milano, Italy

* Corresponding author. Tel. +39 02 2399 3883

E–mail address: fabio.inzoli@polimi.it

Abstract

We provide a probabilistic assessment of CO_2 storage capacity in major sedimentary basins in China. Our approach embeds constraints associated with the increase of reservoir pore pressure due to injection of CO_2 in the presence of resident brine. Pressure build-up must be limited to avoid fault reactivation, caprock failure, and possible leakage, resulting in more conservative estimates of CO_2 storage capacity as compared to volumetric estimates.

We rely on a numerical Monte Carlo framework considering uncertainty in the values of reservoir size and major geological formation attributes (i.e., absolute permeability, porosity, and reservoir compressibility). Our work shows that 10 major basins can potentially store, on average, 1350 Gt of CO_2 during the next 30 years (lower and upper quartiles being 1100 and 1700 Gt of CO_2, respectively). This far exceeds the likely amount (up to 175 Gt of CO_2) required to be stored by 2050. Our analysis also suggests that 6 basins (located close to the largest emission areas) can store about 93 Gt (on average) of CO_2 during the next 30 years. Underground carbon storage in China, coupled with other possible solutions, could meet the aims of the Announced Pledges Scenario (International Energy Agency) to mitigate global warming by 2060.

We also perform a global sensitivity analysis to determine how our predictions of storage capacity may be affected by uncertainties in the simulation model input parameters. Moment-based global sensitivity metrics suggest that geological formation attributes are major sources of uncertainty, significantly affecting model outputs and the associated uncertainty.

Keywords: geological carbon storage; storage capacity; climate change; uncertainty quantification; Global Sensitivity Analysis.

LIST OF MEAN SYMBOLS and NOMENCLATURE

A	Reservoir area	[km^2]
B_o	Oil formation volume factor	
$AMAE_{\theta_i}^{Y}$	Sensitivity index of parameter θ_i for the mean of Y	
$AMAV_{\theta_i}^{Y}$	Sensitivity index of parameter θ_i for the variance of Y	
$AMA\gamma_{\theta_i}^{Y}$	Sensitivity index of parameter θ_i for the skewness of Y	
C	Cohesion parameter	[MPa]
c	Reservoir compressibility	[Pa^{-1}]
d	Inter-well distance	[km]
$\boldsymbol{g}$	Gravity vector	
H	Reservoir thickness	[m]
k	Absolute permeability	[m^2]
ϵ	Ratio between minimum and maximum effective stress	
M_{CO2}	Mass of CO_2	[Gt]
N_P	Number of uncertain model parameters	
n	Number of wells	
p_0	Pressure at the top of the reservoir	[MPa]
Δp	Pressure buil-up	[MPa]
Δp_r	Pressure build-up for reference flowrate	[MPa]
Δp_M	Maximum pressure build-up	[MPa]
Q	Volumetric flowrate	[m^3/s]
Q_M	Maximum flowrate	[Gt/y]
Q_M^{tot}	Total injection flowrate	[Gt/y]
Q_r	Reference flowrate	[Gt/y]

l	Number of MC realizations	
r	Distance from injection well	[m]
r_0	Well radius	[m]
R	Radius of influence of the well	
S	Fracture pressure indicator	[MPa]
t	Time	[y]
T_0	Representative reservoir temperature	[^oC]
$U_{\theta i}^-$, $U_{\theta i}^+$	Support range of θ_i	
$\boldsymbol{Y}$	Vector of model output	
$V(B_i)$	CO_2 storage capacity of the basin B_i	[Gt]
ε	Binary operator	
Ψ	Radius of a fictious equivalent vertical interface	[m]
μ_c	Viscosity of CO_2	[Pa s]
μ_w	Viscosity of brine	[Pa s]
$\boldsymbol{\theta}$	Vector of uncertain model parameters, with entries θ_i	
$\widetilde{\boldsymbol{\theta}}$	Sample of $\boldsymbol{\theta}$	
ρ_{co2}	Density of CO_2	[kg/m^3]
$\sigma_1, \sigma_2, \sigma_3$	Principal stresses	[MPa]
σ_n	Normal stress	[MPa]
τ	Shear stress	[MPa]
ϕ	Porosity	
CCS	Carbon Capture and Storage	
CEC	China Electricity Council	
APS	Announced Pledges Scenario	

IEA	International Energy Agency
GSA	Global Sensitivity Analysis
KLD	Kullback-Leibler Divergence
MC	Monte Carlo
pdf	Probability density function

1. Introduction

China currently accounts for 27% of global CO_2 emissions (IEA, 2021). It has been the most rapidly growing major economy since 1980, its gross domestic product (GDP) having increased more than 30 times. While promoting an impressive growth in renewables and hydropower since 2000, there is still a marked dependence on fossil fuels. These were documented to meet around 85% of its total primary energy needs in 2020 (coal accounting for almost 60% and oil for about a fifth; CEC, 2021). China's emissions from the energy sector (fuel combustion and industrial processes) made up almost 90% of total internal greenhouse gas emissions, compared to 60% in the rest of the world. Hence CO_2 emissions in China reflect a carbon-intensive energy sector. About 70% of China energy-related emissions in 2020 are associated with coal, 12% with oil, 6% with natural gas, and about 11% with process emissions (IEA, 2021; FAO, 2021; Saunois et al., 2020; Friendlingstein et al., 2020; UNFCCC, 2021; He et al., 2020).

Carbon Capture and Storage (CCS) is expected to potentially provide significant support in the reduction of emissions (Celia, 2017; Leung et al., 2014), while considering that additional emissive plants might be developed in the future years. Indeed, considering the dependence of China on fossil fuels, this is an essential technology to achieve net zero CO_2 emissions by 2050 or 2060.

Fig. 1 provides a depiction of the main CO_2 emission points in China, together with pipelines which are already present and potential geologic storage formations considered in our study. The north-eastern part of the country is characterized by the presence of most of the storage formations that are located close to sources of CO_2 emissions. The five provinces of Jiangsu, Shanxi, Shandong, Xinjiang, and Guangdong account for nearly 40% of China's coal burning plants (IEA, 2021). Most of these are located in the northern and eastern parts of the country. This geographical proximity, together with the existing pipeline infrastructure, could contribute to saving transportation costs, provided that these formations can provide sufficient storage capacity. Note that offshore reservoirs are not considered in this work since storage in these formations is likely to be more expensive than onshore.

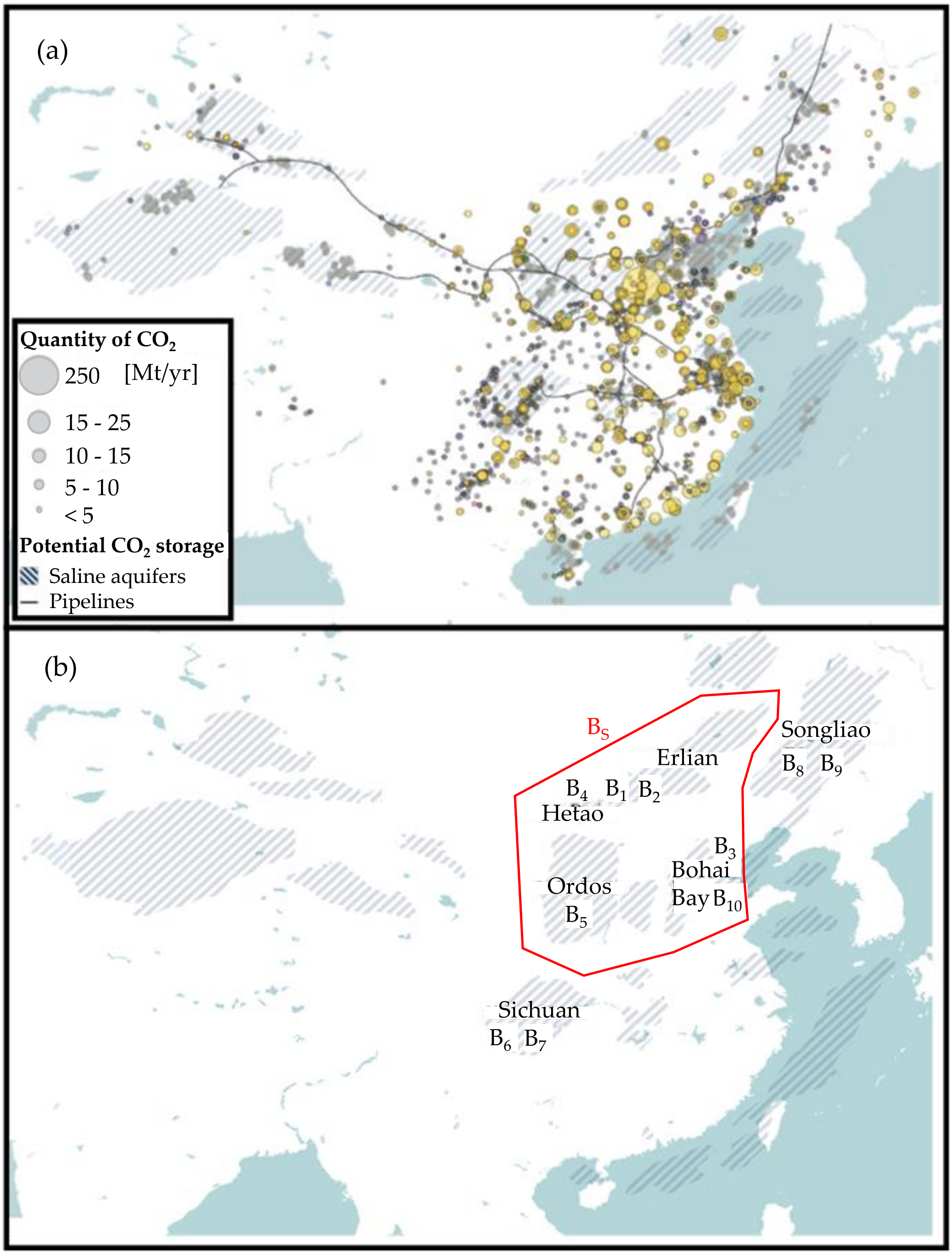

Fig. 1 *Map of (a) major CO_2 sources and (b) potential geological storage basins (denoted as B_1-B_{10}) selected for the analysis of storage CO_2 capacity in China (IEA, 2021).*

An Energy Sector Roadmap to Carbon Neutrality in China is illustrated in IEA (2021). It is then estimated that if the existing emission intensive infrastructure in China continues to operate in the same way it has in the recent years, it could result in 175 Gt of CO_2 emissions between now and 2060 (IEA, 2021). This is equivalent to one-third of the maximum permitted global CO_2 emissions budget (IPCC, 2018) to limit rise in global temperature to 1.5 °C by 2050 (see Mechler et al., 2020 for details).

According to the Announced Pledges Scenario (APS) of the World Energy Outlook (IEA, 2021), China's primary energy demand will grow much slower through 2030 than the overall economy. This is mainly the result of efficiency gains and a shift away from heavy industry. A transforming energy sector leads to rapid improvements in air quality. Solar becomes the largest primary energy source by 2045. Moreover, it is predicted that demand for coal will drop by more than 80% by 2060, oil by around 60%, and natural gas by more than 45%. CO_2 emissions from fossil fuel combustion alone are foreseen to reach around 450 Mt by 2060. They are entirely offset by negative emissions produced by bioenergy in conjunction with carbon capture and storage (BECCS). The APS predicts a growing deployment of CCS in China, reaching 2.6 Gt of CO_2 emissions reduction in 2060. Considering a temporal window of 30 years, this yields a need for almost 80 Gt of cumulative emission reduction to meet the targets.

In this broad context, our objective is to assess the storage capacity (with associated uncertainties) of China to answer the needs of developing CCS projects in the next three decades. To this end, a robust stochastic approach is used to estimate the geological CO_2 storage capacity of 10 major basins (see Fig. 1b) in China and assess if there is sufficient storage capacity to meet the APS targets of CCS for China.

The most suitable formations to establish CO_2 storage projects are deep saline aquifers and depleted oil and gas reservoirs (IEA, 2020). There are various techniques to evaluate CO_2 storage capacity. These are generally comprised within two main groups, depending on whether they are based on (*i*) the evaluation of the gross rock volume or (*ii*) of the pressure build-up across the system (see Section 3 for more details). Several studies use gross rock volume-based techniques (Bachu et al., 2007) to evaluate CO_2 storage capacity in selected regions, basins, and formations in China (e.g., Jiao et al., 2011; Li et al., 2009; Poulsen et al., 2011; Qiao et al., 2012; Vincent et al., 2009; Zhou et al., 2011) and show very high storage capacities. National scale source-sink matching studies show that the storage capacity of onshore aquifers could address the needs of CCS associated with emissions from large, stationary CO_2 point sources in China for several decades (Dahowski et al., 2009).

The works mentioned above mainly focus on a specific region/basin/formation. In this context, our study is set within a broader (national scale) assessment of CO_2 storage capacity in China and a rigorous quantification of associated estimation uncertainties is included. It is further noted that a critical issue associated with most of the available studies is that they solely consider the gross rock volume while neglecting constraints on the rate of injection. The latter can be limited by injection facilities and by the requirement to prevent fracturing the rock, which can in turn lead to escape of the CO_2 intended to be stored. Ignoring pressure constraints can result in overestimation of the reservoir storage capacity. Our study then relies on an integrated assessment model that considers overpressure at each well as a key constraint parameter.

Our work focuses on the assessment of the available capacity of CO_2 storage across 10 selected onshore basins. These encompass oil and gas fields and saline aquifers and are considered to be some of the most suitable sites in China (Wei et al., 2013). We collect information regarding the geophysical characteristics of the selected fields. Since the main traits and attributes of subsurface systems are always affected by uncertainty, a rigorous uncertainty quantification of the storage capacity is performed. As stated above, a stochastic approach is applied based on a pressure build-up assessment for the evaluation of storage capacity across the basins studied. The analyses are framed in a numerical Monte Carlo context. This relies on modern Global Sensitivity Analysis (GSA) techniques to (*a*) quantify the relative importance on storage capacity of each uncertain parameter associated with our simulation model and (*b*) identify the most critical variables affecting the results of the study.

Our workflow is motivated by the observation that understanding the effects of the uncertainty associated with the values of input parameters on the variability of the output of an interpretive model helps to identify the most influential parameters with respect to the model responses (Muleta and

Nicklow, 2005; Pappenberger et al., 2008; Wagener et al., 2009; Ruano et al., 2012; Hill et al., 2016; Ranaee et al., 2021a) while other parameters can be set at prescribed values without distorting the results (Degenring et al., 2004; van Griensven et al., 2006; Chu et al., 2015; Punzo et al., 2015; Nossent et al., 2011). Most applications of GSA rely on variance-based indices (e.g., Sudret, 2008) to quantify the sensitivity of the response(s) of the system to variations in the values of the controlling variables. Recently, Dell'Oca et al. (2017) developed a technique where the influence of uncertain model parameters on various (statistical) moments of a target model output can be quantified through a moment-based GSA approach. Sensitivity is defined by these authors as the average variation of key statistical moments of the probability density function of an output due to model parameter variability. Model parameter uncertainty is then propagated to a target model output (i.e., CO_2 storage capacity) through a Monte Carlo scheme.

The work is organized as follows. Section 2 provides a brief overview of current CCS activities in China. Section 3 introduces the mathematical model to evaluate the carbon storage capacity as well as the stochastic analysis underpinning our results. Implementation of the workflow and the ensuing results are discussed in Section 4. Concluding remarks are presented in Section 5.

2. CCS in China

Development of carbon capture and storage technologies in China is still in the early stages. About 21 pilot, demonstration or commercial projects are currently in operation in China. These are characterized by a combined capture capacity of more than 2 Mt/y of CO_2, most of these being associated with CO_2 - Enhanced Oil Recovery (EOR). The largest of these is possibly the commercial 600 kt/y China National Petroleum Corporation (CNPC) CO_2-EOR project at Jilin, capturing CO_2 from natural gas processing. These CCS projects are located in northern and eastern China where there is a high density of coal-based chemicals and power production as well as good opportunities of performing CO_2-EOR.

Modern CO_2-based enhanced oil recovery (CO2-EOR) processes can assist in mitigating CO_2 emissions. These yield a net reduction in carbon emissions from captured sources while improving hydrocarbon production and (at least partially) revitalizing depleted oilfields. Oil production through CO2-EOR is typically characterized by a less than average carbon intensity/footprint (Cooney et al., 2015).

Bruce Hill et al. (2020) provide a comprehensive overview of key CO2-EOR projects across China. These authors note that China's CO2-EOR projects are typically confined to commercial projects of limited size, test or huff-n-puff injections associated with tens of thousands of tonnes per year, a strategy for recapture or recycle the produced CO_2 not yet being implemented. They also note that China's 2019 roadmap for Carbon Capture, Utilization and Storage (CCUS) sets out goals with the aim of moving CO_2 use from a research stage towards an industrial implementation scenario.

The potential for CO2-EOR in China has been preliminarily assessed by Advanced Resources International, with an estimate that implementation of CO2-EOR would lead to an incremental production of 1 billion barrels of oil following the use of 4 Gt of captured industrial CO_2 (Godec, 2011; Wei et al., 2015).

It is also noted that scarcity of water in China's arid oilfields have hampered waterflooding-based EOR projects and has motivated research and development towards the use of CO_2, which is also favored considering the accessibility of substantially pure CO_2 from industrial sources (Bruce Hill et al., 2020). The potential of enhanced water recovery methods in combination with CO_2 injections is also being currently assessed. The latter is a saline geologic sequestration method and, when combined with reverse osmosis, might enhance availability of water resources in the areas of coal chemical industry and across petroleum basins in China (Li et al., 2019).

A critical element hampering the development and systematic implementation of enhanced oil recovery is related to the observation that the geological settings associated with China's depleted reservoirs typically require fracture stimulation to increase permeability and lead to an established commercial production. Thus, this can severely dampen potential benefits stemming from CO2-EOR projects in China. Zhang et al. (2015) provide some insights on the results of a monitoring campaign performed between 2008 and 2012 for the Jilin EOR project. The authors observed a breakthrough of CO_2 in nearby production wells that approximately amounts to 20%. Ma et al. (2018) analyzed the

CO2-EOR project in Sinopec's Gaoqing 89 block and reported that almost all of the CO_2 injected into the reservoir is vented from the produced oil.

CCS in China is expected to be critical to reach net zero and avert dangerous global warming. To this aim, an all-around evaluation of conservative storage capacity coupled with an understanding of the associated estimation uncertainties can effectively assist decision making for matching CO_2 emission sources with sites of potential storage. In Section 4 we address the way storage capacity of the basins introduced in Fig. 1b can answer the needs of CCS in China.

3. Materials and Methods

Our assessment of the overall storage capacity of a target formation rests on the methodology developed by De Simone and Krevor (2021). The latter explicitly embeds constraints associated with the increase of reservoir pore pressure due to injection of CO_2 in the presence of resident brine (see also e.g., Bachu, 2008; Rutqvist, 2012). It is noted that alternative, volumetric-based techniques for the assessment of storage capacity currently consider at best crude approximations of pressure build-up. Accordingly, such techniques may be less conservative because they do not consider constraints due to reservoir pressurization and possible plume migration through leakage pathways (Szuluczewski et al., 2012).

Our estimates of the largest viable well injection rate and reservoir storage capacity used the open-source software CO2BLOCK (De Simone and Krevor, 2021). A variety of injection scenarios were considered expressed in terms of number of wells and inter-well spacing. This approach has been used recently to assess storage capacity in the North Sea (Karvounis and Blunt, 2021).

The workflow we consider for the assessment of CO_2 storage capacity is depicted in Fig. 2. For simplicity, and consistent with the aim of our overall/global assessment, we assume (*i*) the reservoir to be conceptualized as a homogeneous system and (*ii*) n vertical injection wells to be placed across the domain. Wells are characterized by uniform spacing and operate at the same (constant) volumetric injection rate.

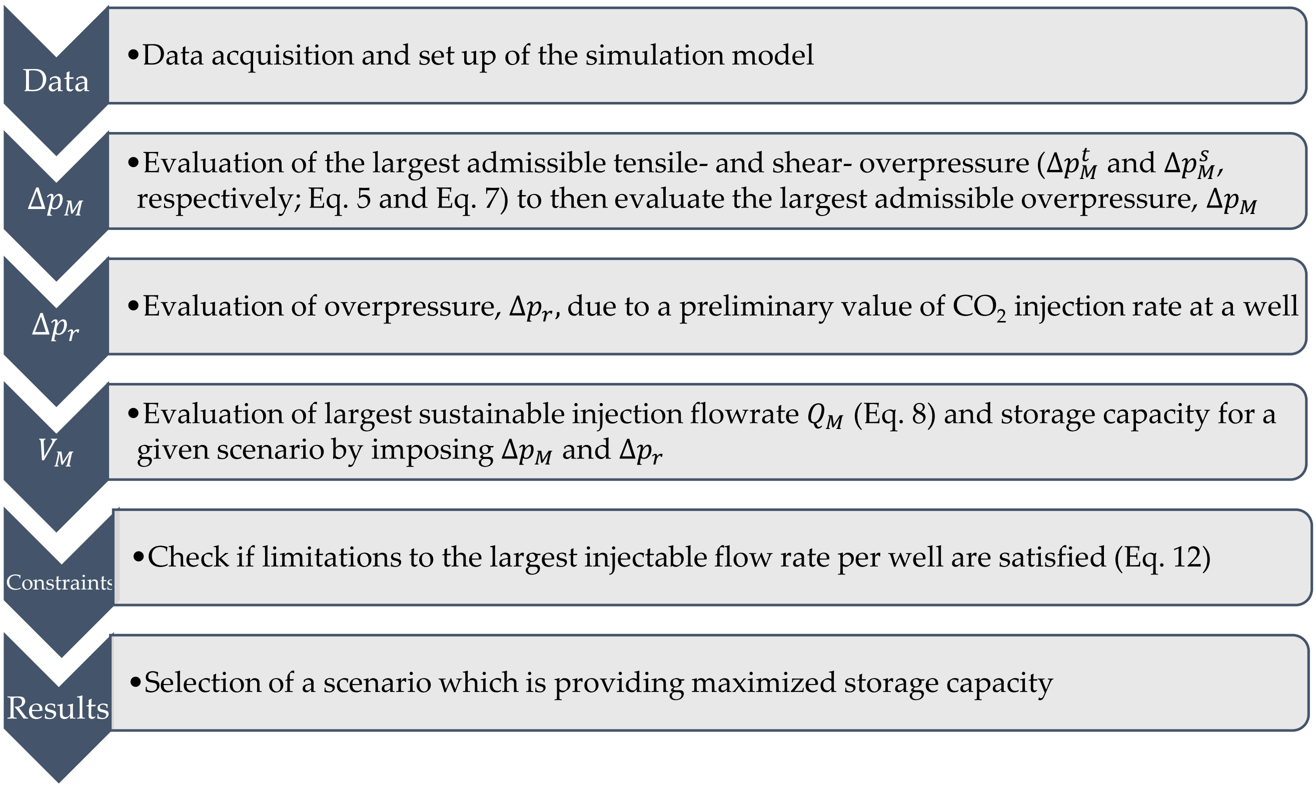

Fig. 2 *Workflow of the analysis to assess the overall CO_2 storage capacity of a reservoir (De Simone and Krevor, 2021).*

3.1.1 Pressure build-up due to single-well CO_2 injection

The study follows De Simone and Krevor (2021) and starts by considering the action of a single injection well and evaluate pressure build-up in the reservoir following injection of a reference CO_2 rate across a given time window. This result will then be used to evaluate the maximum possible injection rate.

From De Simone and Krevor (2021), pressure build-up following CO_2 injection from a single well into a homogeneous reservoir with open boundaries and under the assumption of no pre-existing fractures and negligible trapping can be evaluated as:

$$\Delta p(r,t) = \frac{Q\mu_w}{2\pi kH} \cdot \begin{cases} \dfrac{\mu_c}{\mu_w} \ln\dfrac{\psi}{r} + \ln\dfrac{R}{\psi}, & r \le \psi \\ \ln\dfrac{R}{r}, & \psi < r < R \\ 0, & r \ge R \end{cases} \tag{1}$$

here, $\Delta p(r,t)$ is overpressure (or pressure build-up) at time t and radial distance r from the injection well operating at volumetric flow rate Q; k, ϕ, and H are absolute permeability, porosity, and average thickness of the reservoir, respectively; μ_w and μ_c are brine and CO_2 dynamic viscosity, respectively; $\psi(t)$ represents the radius of an equivalent vertical sharp interface between the injected plume and the resident fluid, which can be expressed as $\psi = \exp(\omega)\xi$ (where $\omega = \frac{\mu_c+\mu_w}{\mu_c-\mu_w}\ln\sqrt{\frac{\mu_c}{\mu_w}} - 1$; $\xi = \sqrt{\frac{Qt}{\pi\phi H}}$); and R corresponds to the well radius of influence. The latter can be assessed according to (Cooper and Jacob, 1946):

$$R = \sqrt{\frac{2.25kt}{\mu_w c}} \quad (2)$$

where c is reservoir compressibility. Equation (1) was introduced by De Simone and Krevor (2021; see their Equation (S1) in their Supplementary Material) and has then been recently employed by Karvounis and Blunt (2021) in their analyses. It stems from the formulation first introduced by Nordbotten et al. (2015; see their Equation (11)) after (*i*) integration across three regions around the injection well where all fluid is CO_2, CO_2 and water are mixed, and all fluid is pure water, respectively, and then (*ii*) introducing an appropriate formulation for the vertical interface between fluids (see also Villarasa et al., 2010).

The action of multiple wells can then be expressed through superposition, i.e.,:

$$\Delta p_{sup}(\boldsymbol{x}_i, t) = \sum_{j=1}^{n} \Delta p(d_{ij}, t) \quad (3)$$

where n is the number of wells, d_{ij} being the distance between wells at (vector) locations $\boldsymbol{x}_i$ and $\boldsymbol{x}_j$ ($\boldsymbol{x}_i$ denoting the vector of spatial coordinates of well i). De Simone and Krevor (2021) assume no interference of CO_2 plumes related to each of the injection wells, (i.e., $d_{ij} > \psi,\ \forall j$). They also suggest that the overpressure at a location $\boldsymbol{x}_i$ of well i can be evaluated through superposition as:

$$\Delta p_{sup}(\boldsymbol{x}_i, t) = \frac{Q\mu_w}{2\pi kH}\left[\frac{\mu_c}{\mu_w}\ln\left(\frac{\psi}{r_0}\right) + \ln\left(\frac{R}{\psi}\right) + \sum_{j=2}^{n}\ln\left(\frac{R}{d_{ij}}\right)\right] \tag{4}$$

where r_0 is well radius (we recall that each well is characterized by the same injection rate Q). This approach allows various scenarios comprising a variety of well numbers and inter-well spacing to be evaluated for a total given injection rate into a reservoir.

3.1.2 Limits to pressure build-up

Pressure build-up must be kept below a critical value, corresponding to the largest pressure, Δp_M, sustainable by the system. Jaeger et al. (2009) showed that formation failure may take place in either a tensile or a shear mode. The former state can take place along planes normal to the minimum principal stress, hereafter termed σ_3 (i.e., $\sigma_1 \geq \sigma_2 \geq \sigma_3$, subscripts being related to the principal directions of the local stress tensor) when pore pressure exceeds the sum of σ_3 and the rock tensile strength, S_0. Thus, the limit value of pressure build-up (Δp_M^t) for a tensile fracturing scenario is:

$$\Delta p_M^t = \sigma_3 - p_0 + S_0 \tag{5}$$

where p_0 is the initial pressure at the top of the reservoir (which is typically considered to correspond to hydrostatic pressure).

Formation failure due to occurrence of high shear can be assessed on the basis of the Mohr-Coulomb failure criterion as:

$$\tau - [C + (\sigma_n - p)tan\varphi] \geq 0 \tag{6}$$

Here, τ is shear; σ_n is the stress normal to the failure plane direction; φ is the angle of internal friction of the formation; and C is cohesion (i.e., intrinsic shear strength). Assuming that failure takes place along planes at angles of $(45^\circ \pm \frac{\varphi}{2})$ with the direction of the largest principal stress, σ_1, the limit pressure build-up (Δp_M^s) for a shear mode scenario is evaluated as:

$$\Delta p_M^s = \frac{\epsilon - \theta}{1 - \theta}(\sigma_1 - p_0) + C \cdot cotan(\varphi) \tag{7}$$

where $\epsilon \leq 1$ is the ratio between the lowest and the largest effective stress values, i.e., $\epsilon = (\sigma_3 - p_0)\,/(\sigma_1 - p_0)$, and $\theta = (1 - sin\varphi)/(1 + sin\varphi)$.

It is noted that a shear-related failure is typically expected in the presence of cohesionless rock systems (corresponding to $C = 0$). Otherwise, when considering reservoirs mainly characterized by cohesive rocks, tensile failure is more common at shallow depths while shear-related failure can take place at large depths. The largest sustainable overpressure (Δp_M) is then evaluated as the lowest between tensile- and shear-related failure pressure values (i.e., Equations (5) and (7)). We emphasize that quantification of these values is plagued by uncertainty due to a variety of sources. These include, for instance, the conceptual description of the system underlying the mathematical representation (Equations (5) to (7)) as well as the associated parametrization which typically embeds uncertain model parameters. Here, we focus on the effect of model parameter uncertainty while relying on the modeling approach described above, which is consistent with the typical nature of a global assessment CO_2 storage capacity project of the kind considered.

3.1.3 Pressure build-up for multi-well injection

We adopt Equation (4) to evaluate the overpressure, Δp_r, due to a preliminary value set for the CO_2 injection rate (Q_r) at a well. Such a value is taken as a reference and is maintained constant across a given temporal window. We do so for a well located in the middle of the reservoir surface area (where overpressure is typically highest). Here, a software default value of $Q_r = \frac{M_0}{\rho_c \cdot n}$ is considered, M_0 and n respectively being the value of total rate injected in the system and the number of wells considered for such a reference scenario. Due to the lack of available data, values of hydrostatic gradient (10 [MPa/km]), temperature gradient (33 [°C/km]), ratio between minimum and maximum effective stress (ϵ = 0.7), and water salinity (1.8×10^5 ppm) are set to the default values provided by the CO2BLOCK toolkit (De Simone and Krevor, 2021).

Several scenarios are built considering various numbers of wells and inter-well spacing for a given total injection rate into the reservoir. De Simone and Krevor (2021) show that pressure build-up decreases with increasing (*i*) the number of wells, n, and (*ii*) the distance between wells, d_{ij}.

3.1.4 Limits to the maximum flowrate

Once the maximum sustainable overpressure Δp_M is assessed and the overpressure, Δp_r, associated with the reference injection rate, Q_r, is evaluated, one can then evaluate the largest sustainable injection flowrate (Q_M) into each well. In this context, De Simone and Krevor (2021) suggest the following formulation to evaluate Q_M, given the response (in terms of overpressure) for a reference scenario:

$$Q_M(t) = -\frac{Q_r \widetilde{\Delta p_M}}{W(-\widetilde{\Delta p_M} e^{-\widetilde{\Delta p_r(t)}})} \tag{8}$$

where W denotes the Lambert function (e.g., De Simone and Krevor, 2021; Corless et al., 1996) for $-\widetilde{\Delta p_M} e^{-\widetilde{\Delta p_r(t)}} < 0$; $\widetilde{\Delta p_M}$ and $\widetilde{\Delta p_r}$ are evaluated as:

$$\widetilde{\Delta p_M} = \frac{\Delta p_M}{b Q_r} \tag{9}$$

$$\widetilde{\Delta p_r} = \frac{\Delta p_r}{b Q_r} \tag{10}$$

where $b = \frac{\mu_w - \mu_c}{4\pi\kappa H \rho_c}$, and ρ_c is the density of CO_2.

Evaluation of the storage capacity for a given time t, i.e., $V_M = ntQ_M$, is then straightforward. Finally, V_M for multiple scenarios is assessed encompassing various numbers of wells and inter-well distances to identify the maximum possible overall capacity of the reservoir.

3.1.5 Technical constraints

Given the scale and nature of the study, and consistent with Karvounis and Blunt (2021), each reservoir is assumed as homogeneous, with wells placed on a Cartesian grid and all operating with the same (constant) injection rate (Q_M). Similar to Karvounis and Blunt (2021), for a given set of model input parameters (see also Section 3.2) we (*a*) generate a range of scenarios associated with various injection well numbers and inter-well distances and (*b*) identify the scenario which maximizes reservoir storage capacity, V_M.

In doing so, we follow De Simone and Krevor (2021) and consider a lower and an upper limit to the distance between well pairs *i* and *j*. The lower limit is set to minimize interference between CO_2 plumes as:

$$d_{i,j} > \sqrt{\frac{tQ_M(t)}{n\pi\phi H\rho_c}} \tag{11}$$

The upper limit is related to the reservoir surface area, A. The latter constraint is rendered as

$$d_{i,j} \leq \sqrt{\frac{A}{n}} \tag{12}$$

Moreover, one could consider the presence of technical (engineering) limitations to the largest injectable flow rate per well (hereafter termed Q_s), so that:

$$n \geq \frac{Q_M^{tot}}{Q_s} \tag{13}$$

where Q_M^{tot} is the total injection rate, corresponding to the sum of the rates injected through the n wells. Scenarios that do not satisfy technical constraints of (11)-(13) are not retained.

Note that, in line with De Simone and Krevor (2021), we set Q_s = 5 Mt/y per well. This is also consistent with the study of Michael et al. (2011), who document that value of Q_s range between 4 and 20 Mt/y across the collection of industrial-scale CO_2 geological storage projects they reviewed.

3.2. Global Sensitivity Analysis and Uncertainty Assessment

Results of simulations of CO_2 storage practices may vary depending on uncertainties in the values of the parameters embedded in Equations (1) to (13). Quantifying the way uncertainties associated with model parameters propagate to model outputs (which are then ultimately employed to estimate the maximum CO_2 storage capacity) can identify the most influential model parameters with respect to the target model response. It can also address the viability of setting some parameter(s) (which are deemed as uninfluential) at prescribed value(s) without significantly affecting the model results. In this sense, sensitivity analysis is a convenient framework to diagnose the behavior of a given model in response to uncertainty associated with its parameters.

The parameters related to the reservoir size (A and H) and formation properties (ϕ, k and c) included in the mathematical formulations presented in Section 3.1 are considered as uncertain. For the purpose of our application, uncertainties linked to CO_2/brine properties (e.g., density and viscosity) are neglected. A vector $\boldsymbol{\theta}$ whose entries θ_i (i = 1, …, N_P) correspond to the values of these N_P = 5 uncertain model parameters is introduced.

The study relies on modern Global Sensitivity Analysis approaches to diagnose the behavior of the model we consider in the presence of parametric uncertainty. We do so by focusing on the maximum CO_2 storage capacity of a target reservoir, $Y = V(B_j)$, and quantify the relative contribution of each uncertain model parameter to the uncertainty of Y.

We rely on random sampling the parameter space of variability $\boldsymbol{\Gamma} = \Gamma_{\theta_1} \cdot \ldots \cdot \Gamma_{\theta_{N_P}}$, Γ_{θ_i} being the support (range of variability) of parameter θ_i, which is viewed as a random quantity (see, e.g., Saltelli et al., 2008; Muleta and Nicklow, 2005; Dell'Oca et al., 2017; Bianchi Janetti et al., 2019; Russian et al., 2019; Ranaee et al., 2021a; 2021b and references therein for additional details).

We focus on the recent moment-based global sensitivity metrics introduced by Dell'Oca et al. (2017). These are denoted as AMA indices and are defined as:

$$AMAE_{\theta_i}^{Y} = \begin{cases} \dfrac{1}{|E[Y]|} E[|E[Y] - E[Y|\theta_i]|] & if \quad E[Y] \neq 0 \\ E[|E[Y|\theta_i]|] & if \quad E[Y] = 0 \end{cases} \tag{14}$$

$$AMAV_{\theta_i}^{Y} = \frac{E[|V[Y] - V[Y|\theta_i]|]}{V[Y]} \tag{15}$$

$$AMA\gamma_{\theta_i}^{Y} = \begin{cases} \dfrac{1}{|\gamma[Y]|} E[|\gamma[Y] - E[Y|\theta_i]|] & if \quad \gamma[Y] \neq 0 \\ E[|\gamma[Y|\theta_i]|] & if \quad \gamma[Y] = 0 \end{cases} \tag{16}$$

where $AMAE_{\theta_i}^{Y}$, $AMAV_{\theta_i}^{Y}$, and $AMA\gamma_{\theta_i}^{Y}$ represent the sensitivity indices associated with the mean, variance, and skewness of $Y(\boldsymbol{\theta})$, respectively ($E(\bullet)$ denotes expected value, $V(\bullet)$ denotes variance and $\gamma(\bullet)$ is skewness). Note that indices $AMAE_{\theta_i}^{Y}$, $AMAV_{\theta_i}^{Y}$ and $AMA\gamma_{\theta_i}^{Y}$ quantify the expected change of mean, variance, and skewness of Y due to variations of θ_i, respectively. The combined use of these indices enables one to perform a comprehensive GSA of the target model response, $Y(\boldsymbol{\theta})$, quantifying the impact of each entry of $\boldsymbol{\theta}$ on the variability of Y. When considered in the context of typically used variance-based methods (such as, e.g., methods based on Sobol indices; Sobol, 1993), this approach provides enhanced understanding on the way uncertain parameters are acting through the model onto key statistical moments characterizing the distribution of the selected model output.

Considering that probability densities of the values of a reservoir storage capacity can be different from a classical normal distribution, relying on a traditionally used variance-based sensitivity criterion (e.g., Sobol, 1993) may provide an incomplete picture of a system response to uncertainty in model parameters. Instead, moment-based sensitivity metrics of the kind we consider enable one to analyze the system response in terms of its main statistical moments. As seen above, these include the expected value of the simulation response, Y, the spread around the mean, and the degree of symmetry and tailedness of the probability density function (pdf) of Y. These indices allow for a comprehensive description of how the structure of the pdf of Y is affected by variations of uncertain model parameters.

4. Results

4.1. Characteristics of the main sedimentary basins in China

The characteristics of the basins introduced in Fig. 1b are analyzed here for a (preliminary) assessment of suitability for CO_2 storage.

The study of Bruce Hill et al. (2020) is referred for a detailed description of the main geological traits characterizing the lithology of typical continental reservoir rocks across China. Only a brief summary is included here for completeness. Sedimentary reservoirs across China are typically consolidated depositional basins filled with sedimentary sequences from fluvial and lacustrine geologic settings (Petroleum Geology of China, 1992). Key elements associated with these have been driven by burial, compaction, and related diagenetic processes (Bruce Hill et al., 2020). Basins in north-eastern China are chiefly characterized by a marked overall thickness of sedimentary bodies and several sets of reservoir-caprock layers, offering a setting of potential interest for geological storage of captured CO_2 (Zeng et al., 2013). In this scenario, Diao et al. (2017) document that argillite (mudstone and shale) and evaporites (gypsum and rock salt) constitute the most commonly found caprocks for oil and gas fields in China; caprocks formed by carbonate rocks and frozen genesis caps are also found in some fields.

Sandstone reservoir formations in Erlian sub-basins are buried at depths of 1-3 km and potential storage sites are formed by structural and fault traps. Wang et al. (2018) showed that key lithological traits of the Dongying and Shahejie formations in the Bohai bay Basin encompass pebbly sandstone, siltstone, sandstone intercalated with mudstone, and oil shale. Oilfields and surrounding aquifers across the Ordos basin could be considered as a potential target for storage of CO_2, due to the presence of sandstones characterized by a thickness of about 200 m at suitable depths and potential structural and lithological traps. Mudstone interbedded with fine-grained sandstone of the Pliocene Wulantuke formation and mudstone intercalated with fine-grained sandstone and marlite of the Miocene Wuyuan formation form the caprock in the Hetao Basin, silt to medium-grained sandstone of the Oligocene Linhe formation (thickness of 260-340 m) providing a good potential for storage. Saline aquifers in the Sichuan Basin are characterized by an overall very low porosity and permeability. Otherwise, natural gas fields in the Sichuan Basin are characterized by suitable caprock conditions for CO_2 storage (Diao et al., 2017). The reader is referred to the work of Sun et al. (2021) for an exemplary stratigraphy of the Sichuan Basin. Su et at (2013) performed a (basin scale) assessment of the potential CO_2 storage capacity in the deep saline aquifers of the Songliao Basin. These authors suggest that spatial heterogeneities therein (in terms of e.g., pore volume, temperature, or pressure distribution) pose significant challenges for the quantification of storage potential.

Wei et al. (2013) implemented a GIS-based framework of analysis (first developed by Bachu, 2003) and reported that the basins illustrated in Fig. 1b are potentially suitable for CO_2 storage (due to their makeup, mainly associated with large sedimentary thickness, tectonic stability, and several sets of reservoir-caprock pairs). Their analysis considered four elements: (*i*) storage capacity and injectivity; (*ii*) risk minimization and storage security; (*iii*) environmental restrictions; and (*iv*) economic considerations. It was then shown that 90% of CO_2 sources are within 160 km of a CO_2 storage reservoir. This suggests that the technology is economically feasible (Dahowski et al., 2009).

For the purpose of our analysis, suitable layers within the same formation are conceptualized as different basins (e.g., B_6 and B_7 in Fig. 1b). Basins which are suitable to CO_2 storage and are at the same time close to emissions sources are included in our study (see Fig. 1).

The Erlian basin (see Fig. 1b) is a highly heterogeneous continental basin with generally low permeability and porosity. The Manite and Tengger subbasins belong to the Erlian basin and are denoted as B_1 and B_2, respectively, in Fig. 1b. These include sandstone rich formations with a thickness of the order of hundreds of meters buried at depths of 1-3 km. These elements potentially provide a substantial CO_2 storage potential. Additionally, analysis of potential sources and sinks reveals that marked CO_2 emission point sources (i.e., the Datang Group Hexigten Qi, a coal to gas factory, estimated to emit about 8.56 Mt/y) are located less than 100 km away from these subbasins (Fig. 1a). The Bohai Bay basin (which includes subbasins B_3 and B_{10} in Fig. 1b) contains porous sandstone and conglomerate rich formations. These are sealed by mudstones and lithological and structural traps, thus being associated with potentially favorable conditions for CO_2 storage. The Hebei Kaiyue Chemical Group (with about 4 Mt/y of CO_2 emissions) is located within 50 km from these subbasins. The Hetao basin (B_4 in Fig. 1b) comprises a well-defined succession of mudstone, fine-grained sandstone, marlite, and silt to medium-grained sandstone (with a thickness of 260-340 m). It thus forms an ideal environment for storage of CO_2. Source-sink matching identifies CO_2 emissions from a coal to olefin factory in Baotao City (associated with about 2.4 Mt/y of CO_2 emissions). The Ordos Basin (B_5 in Fig. 1b) is characterized by sequences of sealed reservoir layers, with seemingly good potential for CO_2 storage. Emission sources that can be found in its proximity include the Shenhua Ningxia Coal industry Group (about 3 Mt/y of CO_2 emissions). Furthermore, it is noted that a pilot project with a storage potential of about 1 Mt of CO_2 is already in place (Zeng et al., 2013). Wei et al. (2013) suggest that Ordos (B_5 in Fig. 1b), Sichuan (B_6-B_7 in Fig. 1b), and Songliao (B_8-B_9 in Fig. 1b) basins are the most promising sites for CO_2 aquifer storage projects in China. The Sichuan basins (B_6 and B_7) are approximately in the central part of China. These consist of different reservoir-cap combinations of lenticular sand body capped by brown-red mudstone and sandy mudstone with siltstone layer. They are close to emission sources of about 100 Mt/y overall.

The Songliao basin (B_8 and B_9) is a large sedimentary basin in north-eastern China. It is an important area due to the presence of mineral resources and well-established industrial bases, i.e., it accounts for one-third of the total oil production in China (Su et al., 2013). Sandstone and siltstone with caprocks of low permeable mudstone constitute the main lithology of the potential storage formations. There are several CO_2 sources in the area, i.e., the Northern Songliao basin alone with several sources emitting more than 10 Mt/y of CO_2 (National Bureau of Statistics of China, 2008). Wei et al. (2013) evaluated the Tarim, Junggar, Turman-Hami, and Qaidam basins (all located in of the north-west of China) as suitable sites for CO_2 storage. These are not included in our assessment because of (*i*) their large distances from major emission sources and (*ii*) socio-political concerns that reduce the potential of these basins to firmly establish CO_2 storage projects. Table 1 lists some key characteristics of the selected basins (B_1-B_{10}) collected from prior studies (e.g., Zeng et al., 2013; Diao et al., 2017; Fan et al., 2014; Wang et al., 2014; Jin et al., 2017; Wang et al., 2018). Such information is required for the assessment of carbon storage capacity, following Equations (1)-(13) in Section 3. For the purpose of illustration, Fig. 3 provides a schematic depiction including the main parameters listed in Table 1. The overall thickness of a basin is evaluated across the whole geological formation containing an ensemble of permeable layers (suitable for CO_2 sequestration). Shallowest- and mean-depths of the reservoir are referred to the mean sea level as depicted in Fig 3.

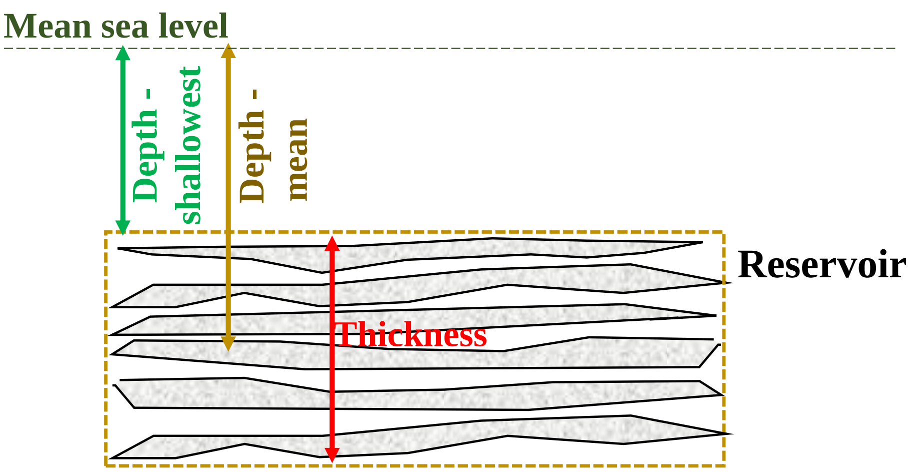

Fig. 3. *schematic illustration of the main parameters listed in Table 1 onshore reservoir characteristics suitable for CO_2 sequestration. The thickness includes only the permeable layers shaded.*

Table 1. *Characteristics of the selected basins (B_1-B_{10} in Fig. 1b).*

Unit name (subbasin)	Depth - shallowest [m]	Depth - mean [m]	Thickness* [m]	Area [km^2]	Permeability [mD]	Porosity [-]
Manite subbasin (B_1)	1000	2000	300	10000	1000	0.15
Tengger subbasin (B_2)	1000	2000	300	12170	1000	0.15
Bohai Xialahoe (B_3)	700	2240	200	428	1550	0.23
Hetao basin (B_4)	1800	2650	300	2000	285	0.175
Ordos basin (B_5)	870	1400	200	150	125	0.184
Sichuan Jurassic (B_6)	3500	3650	300	37000	5	0.1244
Sichuan upper Triassic (B_7)	4000	4500	500	37000	1	0.05
Songliao Yaojia (B_8)	1287	1809	150	260000	200	0.2
Songliao Qingshankou (B_9)	1469	2424	150	260000	210	0.188
Shahejie Formation (B_{10})	1600	2000	300	2500	10000	0.2

** It is noted that the overall thickness (termed thickness, for brevity) of the basin formation is assessed across the whole geological formation and its evaluation encompasses solely the permeable layers without including cap rock and impermeable layers (see also Fig. 3).*

4.2. Uncertainty Assessment

As mentioned in Section 3.2, we select a set of uncertain model parameters θ_i (with i= {1, …,5}). We consider the values of the uncertain parameter to be characterized by uniform probability densities. This modeling choice is consistent with scenarios where prior information (e.g., measurements) on model parameters is not available and enables one to give equal weight to each value across the space of variability of a given parameter. We refer to information reported in the literature (Zeng et al., 2013; Diao et al., 2017; Fan et al., 2014; Wang et al., 2014; Jin et al., 2017; Wang et al., 2018) and consider broad ranges of variability for the values of each uncertain model parameter θ_i (see Table 2). Selection of the support ranges of each θ_i values is set to represent broad ranges of variability based on typical measurement uncertainties (see, e.g., Sifuentes et al., 2009; Li and Liu, 2016; Ajayi et al., 2019; Barros et al., 2021). We set the support of $\theta_1 = H$ and $\theta_2 = A$ considering a ± 50 % and ± 20% range of variability around the corresponding mean values reported in the literature. $\theta_3 = log_{10}(k)$ to vary across the range of ± 1, to encompass a broad range of variability. Porosity is correlated to permeability as $\phi = \alpha\ log_{10}(k)$. We set the values of $\theta_4 = \alpha$ to range across the support ± 0.03 (accounting for possible inaccuracies of the empirical equation used for porosity modeling). Accordingly, the distribution of ϕ corresponds to the product of two uniformly distributed random variables. Sample values of $\theta_5 = log_2(c)$ are described through a uniform distribution within the support range of ± 1 around mean values reported in the literature (see Table 2).

***Table 2** List of the uncertain model parameters. Each uncertain parameter θ_i (i = 1, ..., 5) is characterized by a uniform distribution with support $[U^-_{\ddot{\theta}_i}, U^+_{\ddot{\theta}_i}]$.*

Uncertain parameters	$\theta_1 = H$ [m]	$\theta_2 = A$ [km^2] ×10^3	$\theta_3 = log_{10}(k)$ [k in mD]	$\theta_4 = \alpha$ [-]×10^{-3}	$\theta_5 = log_2(c)$ [c in Pa^{-1}]
	$[U^-_{\ddot{\theta}_1}, U^+_{\ddot{\theta}_1}]$	$[U^-_{\ddot{\theta}_2}, U^+_{\ddot{\theta}_2}]$	$[U^-_{\ddot{\theta}_3}, U^+_{\ddot{\theta}_3}]$	$[U^-_{\ddot{\theta}_4}, U^+_{\ddot{\theta}_4}]$	$[U^-_{\ddot{\theta}_5}, U^+_{\ddot{\theta}_5}]$
Manite subbasin (B_1)	[150, 450]	[8, 12]	[2, 4]	[48, 51]	[-31, -29]
Tengger subbasin (B_2)	[150, 450]	[9.7, 14]	[2, 4]	[48, 51]	[-31, -29]
Bohai Xialahoe (B_3)	[100, 300]	[0.34, 0.52]	[2.2, 4.2]	[70, 75]	[-31, -29]
Hetao basin (B_4)	[150, 450]	[1.6, 2.4]	[1.5, 3.5]	[69, 73]	[-31, -29]
Ordos basin (B_5)	[100, 300]	[0.12, 0.18]	[1.1, 3.1]	[85, 91]	[-31, -29]
Sichuan jurassic (B_6)	[150, 450]	[29, 44]	[0, 2]	[21, 13]	[-31, -29]
Sichuan upper triassic (B_7)	[250, 750]	[29, 44]	[0, 2]	[48, 51]	[-31, -29]
Songliao Yaojia (B_8)	[75, 225]	[210, 310]	[1.3, 3.3]	[84, 90]	[-31, -29]

Songliao Qingshankou (B_9)	[75, 225]	[210, 310]	[1.3, 3.3]	[78, 83]	[-31, -29]
Shahejie Formation (B_{10})	[150, 450]	[2, 3]	[3, 5]	[48, 51]	[-31, -29]

A collection of Monte Carlo (MC) realizations is generated by randomly sampling from the distributions of the uncertain model parameters and the storage capacity of each reservoir j, $V(B_j)$, is evaluated. The total storage capacity, $V(B_{tot})$, is evaluated considering all of the realizations generated across the 10 basins studied. Fig. 4 depicts the way mean, variance, skewness, and coefficient of variation of the values of storage capacity depend on the number of realizations considered. Results for each of the basins are depicted together with those associated with total storage capacity. These results suggest that stability of MC simulation results (in terms of moments of CO_2 storage capacity) is attained after about 5000 MC realizations.

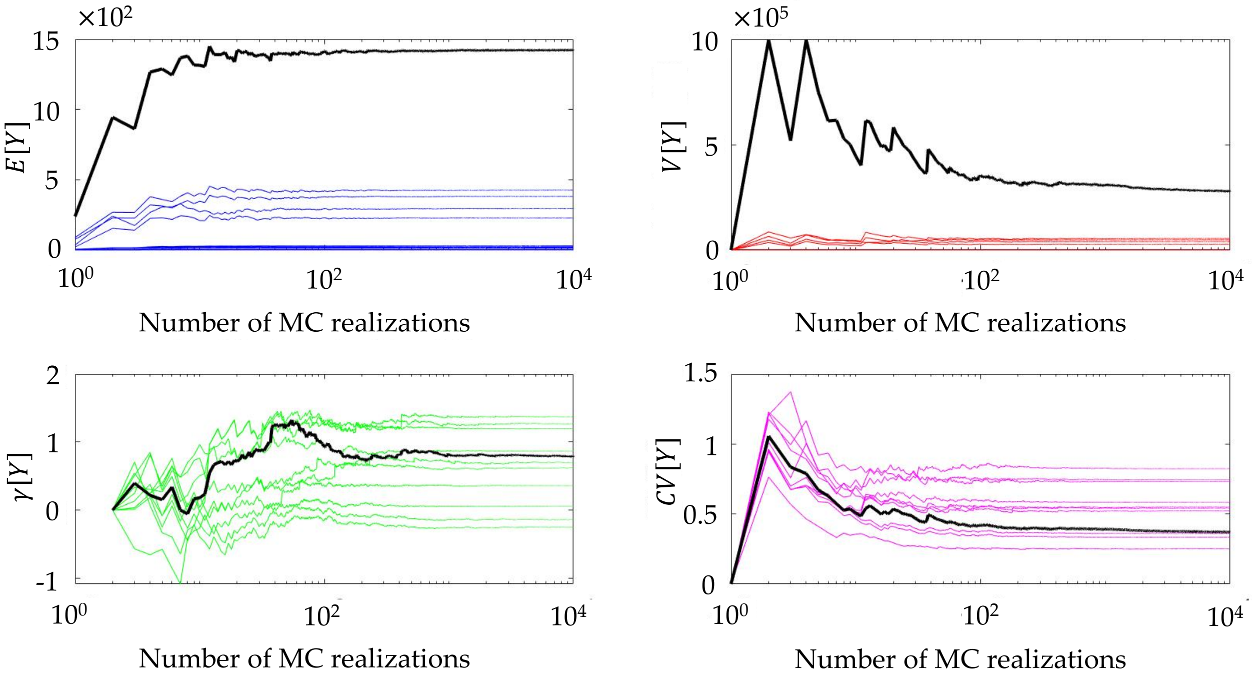

Fig. 4. *Mean ($E[Y]$), variance ($V[Y]$), skewness ($\gamma[Y]$), and coefficient of variation ($CV[Y]$) of the values of storage capacity (i.e., $Y = V(B_j)$) versus the number of MC realizations considered. Results for each of the basins (colored curves; $V(B_1)$ - $V(B_{10})$) are depicted together with those associated with total storage capacity (black curves; $V(B_{tot})$).*

The degree of similarity/difference between two sample probability density functions (pdfs) of the storage capacity evaluated with different numbers of MC realizations is quantified (see Table 3) through the Kullback - Leibler divergence, KLD (Kullback and Leibler, 1951). Note that small values of KLD correspond to small differences between the selected pdfs.

Table 3. *Values of the Kullback - Leibler divergence, KLD, for selected pairs of MC realizations (i.e., 1000 vs 2000, 3000 vs 4000, 5000 vs 6000, 7000 vs 8000, 9000 vs 10000).*

Basin	KLD (l=1000 vs 2000)	KLD (l=3000 vs 4000)	KLD (l=5000 vs 6000)	KLD (l=7000 vs 8000)	KLD (l=9000 vs 10000)
B_1	2×10^{-3}	4×10^{-4}	1×10^{-4}	8×10^{-5}	8×10^{-5}
B_2	3×10^{-3}	8×10^{-4}	2×10^{-4}	2×10^{-4}	1×10^{-4}
B_3	4×10^{-3}	5×10^{-4}	2×10^{-4}	2×10^{-4}	1×10^{-4}
B_4	4×10^{-3}	5×10^{-4}	1×10^{-4}	1×10^{-4}	8×10^{-5}
B_5	4×10^{-3}	1×10^{-3}	4×10^{-4}	2×10^{-4}	1×10^{-4}
B_6	4×10^{-3}	8×10^{-4}	2×10^{-4}	2×10^{-4}	4×10^{-5}
B_7	9×10^{-3}	8×10^{-4}	4×10^{-4}	2×10^{-4}	2×10^{-4}
B_8	3×10^{-3}	7×10^{-4}	3×10^{-4}	2×10^{-4}	2×10^{-4}
B_9	4×10^{-3}	9×10^{-4}	5×10^{-4}	2×10^{-4}	2×10^{-4}
B_{10}	1×10^{-2}	6×10^{-3}	1×10^{-4}	1×10^{-4}	5×10^{-5}
B_{tot}	2×10^{-3}	3×10^{-4}	1×10^{-4}	9×10^{-5}	4×10^{-5}

Overall, the set of analyses performed imbues us with confidence that a number of MC realization approximately equal to 5000 guarantees stable results for the ensuing pdf of the storage capacity for each of the target basins. As a result, 10^4 random Monte Carlo realizations are run for each of the basins considered.

4.3. Sensitivity Analysis

We quantify the sensitivity of the simulated model outputs (i.e., $Y = V(B_i)$) with respect to variations in the values of uncertain parameters, θ_i, referring to the approach introduced in Section 3.2. Figures 5-7 depict values of the AMA indices (Equations (14) - (17)) evaluated for each basin (B_i; i = 1, …, 10) and associated with mean, variance, and skewness of $V(B_i)$ with respect to θ_i.

When considering the mean value of storage capacity (as rendered through $AMAE_{\theta_i}^{Y}$; Equation 13), one can see that all parameters are characterized by the same strength in B_1, B_2 and B_{10}. These are intermediate size basins with reasonably high values of permeability. Reservoir compressibility and the height of the reservoir are instead the most important quantities driving the potential storage capacity of B_8 and B_9 (very large basins with intermediate values of permeability). Otherwise, the intrinsic properties of the geological system appear to be most significant for basins B_3, B_4 and B_5 (small basins with intermediate values of permeability), as well as B_6 and B_7 (large basins with low permeability). These results confirm that formation properties are the key parameters effecting storage capacity for the basins with low permeability values, even as the total volume of the reservoir is large (e.g., B_6, B_7). Equation (4) shows how overpressure is linked to the rock attributes. In such cases, low values of permeability constrain displacement of the resident brine by the injected CO_2. Accumulation of CO_2 can then locally lead to overpressure conditions (Karvounis and Blunt, 2021). It is noted that in the presence of high permeability values the main controlling factors to avoid excessive overpressure are (*a*) the height of the system (which enables accumulation of CO_2) and (*b*) reservoir compressibility (which allows for additional space for CO_2).

With reference to the impact of uncertain model parameters on model output variance, $AMAV_{\theta_i}^{Y}$ (Equation (15)) values show almost the same trend as the corresponding $AMAE_{\theta_i}^{Y}$ for all reservoirs. An exception is given by B_6 and B_7 where, in addition to rock attributes, $AMAV_{\theta_i}^{Y}$ shows also high sensitivities to c (i.e., reservoir compressibility). This can indirectly be linked to the low permeability values associated with these basins. Indeed, low permeability can result in local accumulation of CO_2 and local increases of pore pressures. Hence, high values of CO_2 compressibility can alleviate some effects of low permeable formations on a local increase of pore pressures. Accordingly, basins B_6 and B_7 show higher sensitivity to the values of the parameters directly influencing flow of CO_2 across the system (i.e., ϕ, k, c) due to their extremely low values of permeability and porosity.

Values of $AMA\gamma_{\theta_i}^{Y}$ reveal that skewness is mostly impacted by model uncertain parameters in small basins (i.e., B_1, B_2, B_3), where almost all uncertain parameters are important.

In summary, our results reveal that uncertainty in geological attributes and in reservoir size influence the CO_2 storage capacity of basins with reasonably high values of permeability (i.e., B_1, B_2, B_{10}). Otherwise, system properties (i.e., ϕ and k) appear to be the most important parameters for evaluating storage capacity of the basins with small (to intermediate) values of permeability (B_3, B_4, B_5, B_6, B_7). Reservoir compressibility and the height of the reservoir mainly influence model outputs in very large basins with high values of porosity/permeability (i.e., B_8-B_9).

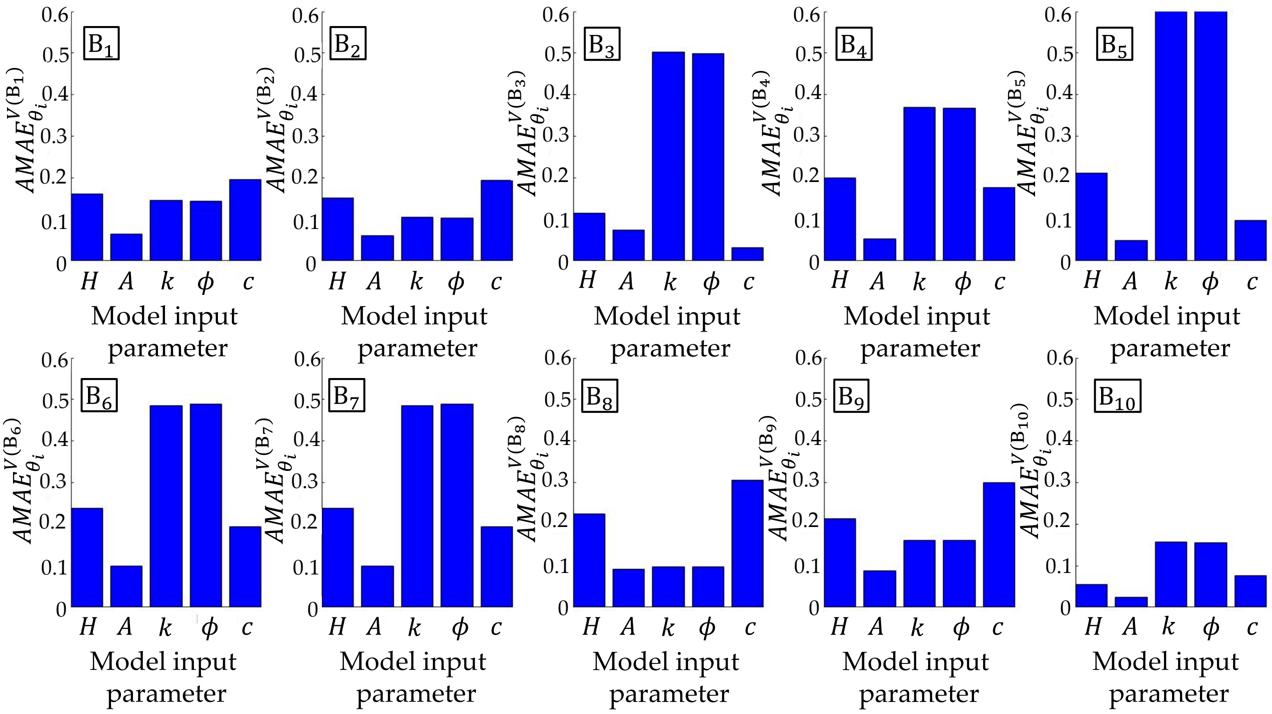

Fig. 5. *Evaluation of the moment-based* $AMAE_{\theta_i}^{Y}$ *indices associated with the mean storage capacity of each basin studied* B_j *(*$j = \{1, \ldots, 10\}$*).*

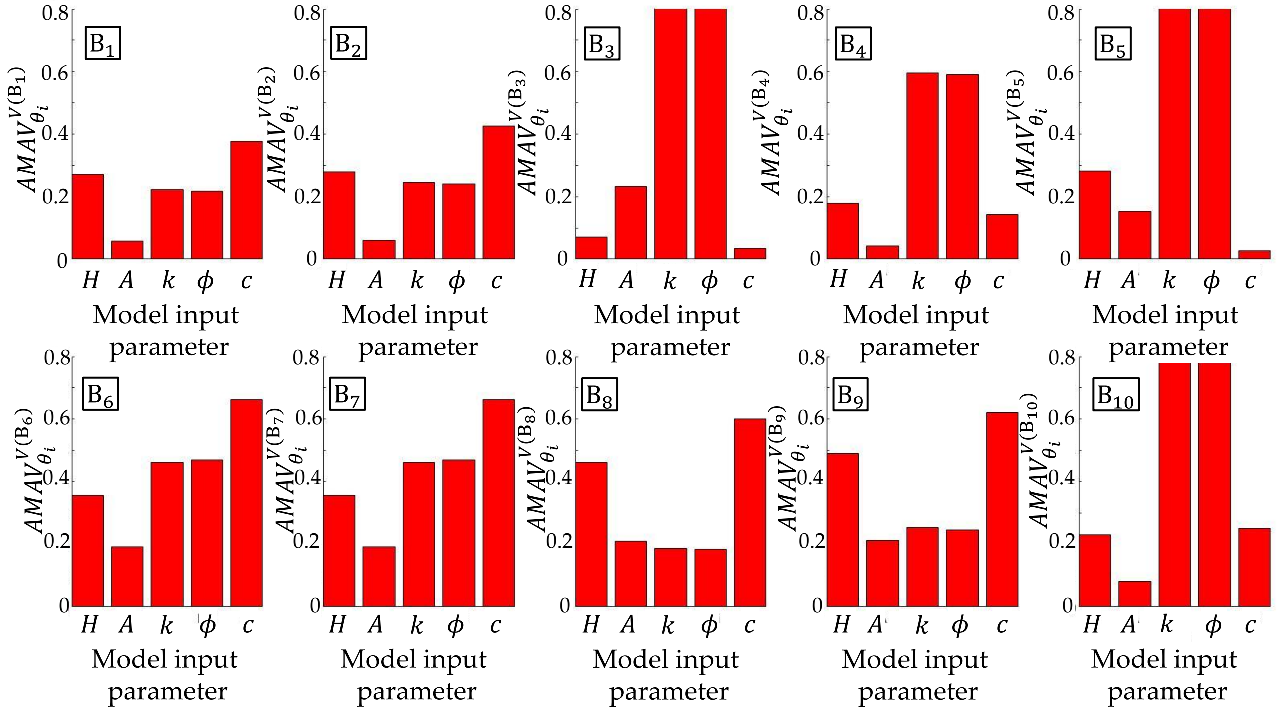

Fig. 6. *Evaluation of the moment-based* $AMAV_{\theta_i}^{Y}$ *indices associated with the variance of the distribution of storage capacity of each basin studied* B_j *(j = {1,…,10}).*

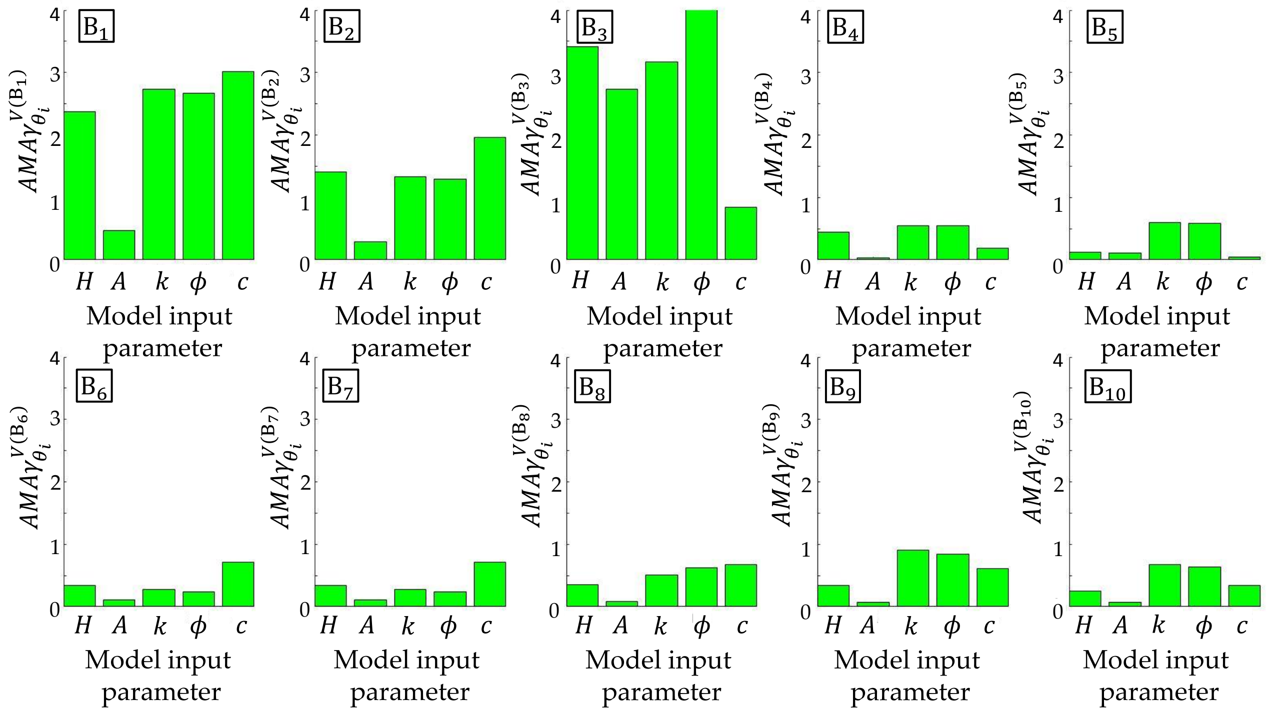

Fig. 7. *Evaluation of the moment-based* $AMA\gamma_{\theta_i}^{Y}$ *indices associated with the skewness in the distribution of storage capacity of each basin studied* B_j *(*$j = \{1,\ldots,10\}$*).*

4.4. Uncertainty Quantification for CO_2 Storage Capacity

Our results illustrate that sample pdfs of the potential storage capacity show remarkable variability across the basins analyzed (see Fig. 8). Sample pdfs of $V(B_j)$ for intermediate size basins with high permeability (i.e., B_1, B_{10}) are typically characterized by almost symmetrical distributions. Distributions associated with small (and highly permeable) basins (i.e., B_3, B_4, B_5) are skewed towards high values of $V(B_j)$. Large and low permeability basins (i.e., B_6, B_7) are characterized by positively- (right-) skewed distributions, with frequent high values of storage capacity. Sample distributions of very large (highly permeable) basins (i.e., B_8, B_9) are positively skewed, with long tails to high values of storage capacity.

The emergence of left-skewed distributions (e.g., B_2) can be related to the constraint imposed to the range of variability of inter-well distances (Equations (11) and (12)). This severely limits the number of wells that can be placed in small reservoirs. Consequently, many realizations are characterized by an estimated storage capacity limited by this constraint, with a tail of less likely smaller capacities limited by other properties (see Fig. 8). Otherwise, the emergence of a right-skewed distribution is mainly driven by the engineering constraints adopted (i.e., Q_s = 5 Mt/y per well). These limit the storage capacity that can be obtained by a given number of wells. Basin B_7 is characterized by a high frequency of low values of $V(B_j)$. It is noted that these values are mainly related to realizations characterized by very low permeability values that are subject to the constraint on permeability (i.e., k > 1 mD) associated with the simulation toolbox (De Simone and Krevor, 2021).

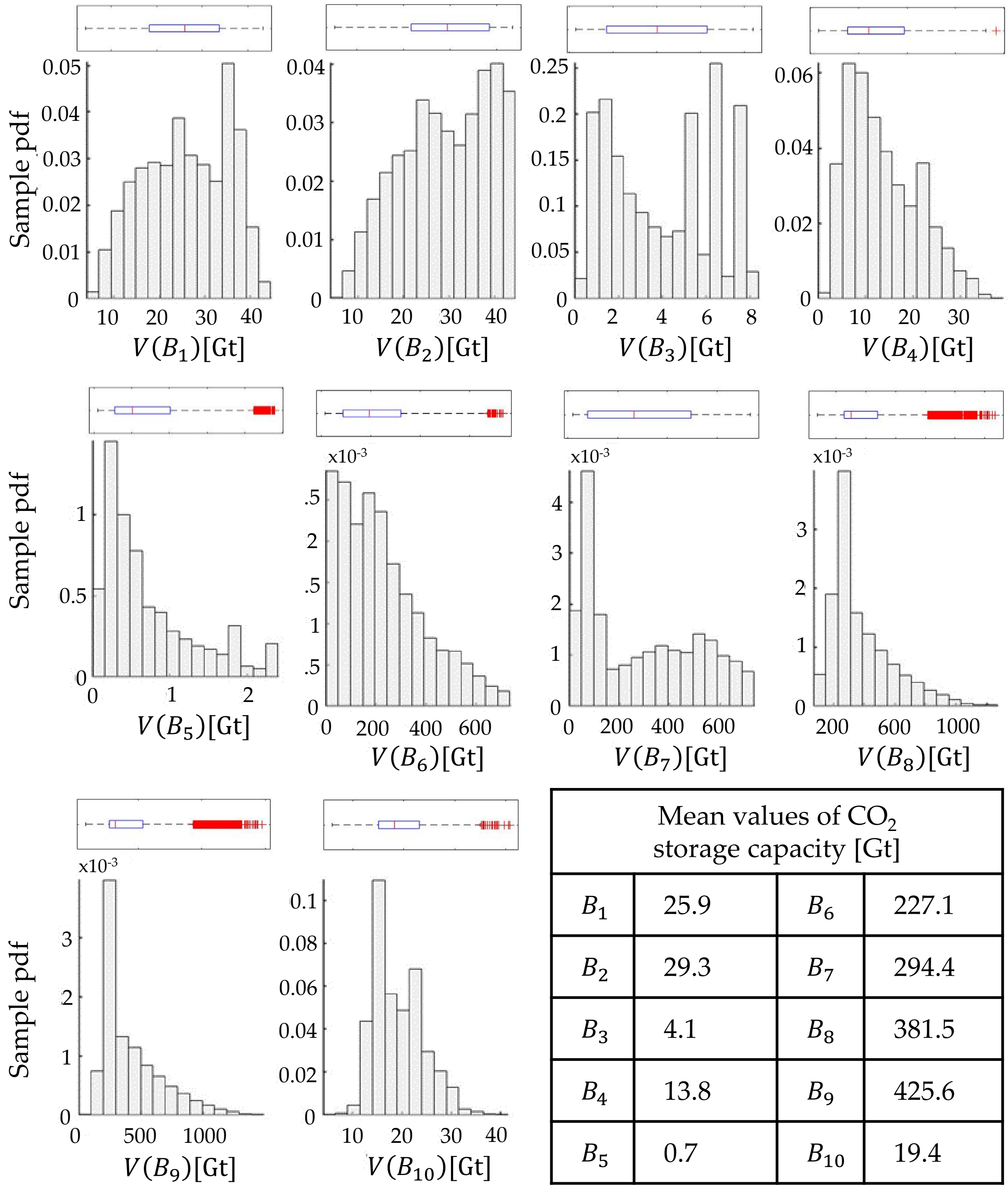

Mean values of CO_2 storage capacity [Gt]			
B_1	25.9	B_6	227.1
B_2	29.3	B_7	294.4
B_3	4.1	B_8	381.5
B_4	13.8	B_9	425.6
B_5	0.7	B_{10}	19.4

Fig. 8. *Sample pdfs of CO_2 storage capacity, $V(B_j)$ (j={1,…,10}) for the basins studied. Results are associated with 10^4 MC realizations.*

One can then relate these probabilistic results to CO_2 emissions documented across nearby regions (Cui et al., 2021). An average (mean) of 55.3 Gt of CO_2 is seen (Fig. 9a) to be potentially stored in 30 years in B_1 and B_2 (associated with the Erlian basin). This value is compatible with accommodating about 16 Gt of CO_2 (in 30 years) of emissions from power and industrial sectors located in the provinces of Beijing and Inner Mongolia. An average value of 13.8 Gt of CO_2 potential storage capacity is associated with the Hetao basin (i.e., B_4). This can satisfy the storage needs in the Gansu and Ningsia provinces, corresponding to about 10 Gt of CO_2 in 30 years (Cui et al., 2021). Fig.9b shows that the Bohai Bay basin (encompassing B_3 and B_{10}) can serve (in an average sense) 23.4 Gt of CO_2 storage capacity in 30 years. This basin is close to the Tianjin, Shandong, Jiangsu, Shanxi, Henan, and Hebei provinces. These provinces are estimated to be characterized by a cumulative emission of about 82 Gt of CO_2 by 2050 (Cui et al., 2021). Accordingly, underground storage could only partially satisfy the projected requirements in this region. Thus, one would need to either design a proper management scheme for (*a*) transporting some parts of the captured CO_2 to other basins or (*b*) combining applications of CCS with fossil free and renewable power generation. It is estimated that the Shaanxi, Hubei and Qinghai provinces will produce almost 20 Gt of CO_2 in the next 30 years. Our results show that the nearby Ordos basin (i.e., B_5) cannot satisfy the totality of the needs of carbon storage in this region.

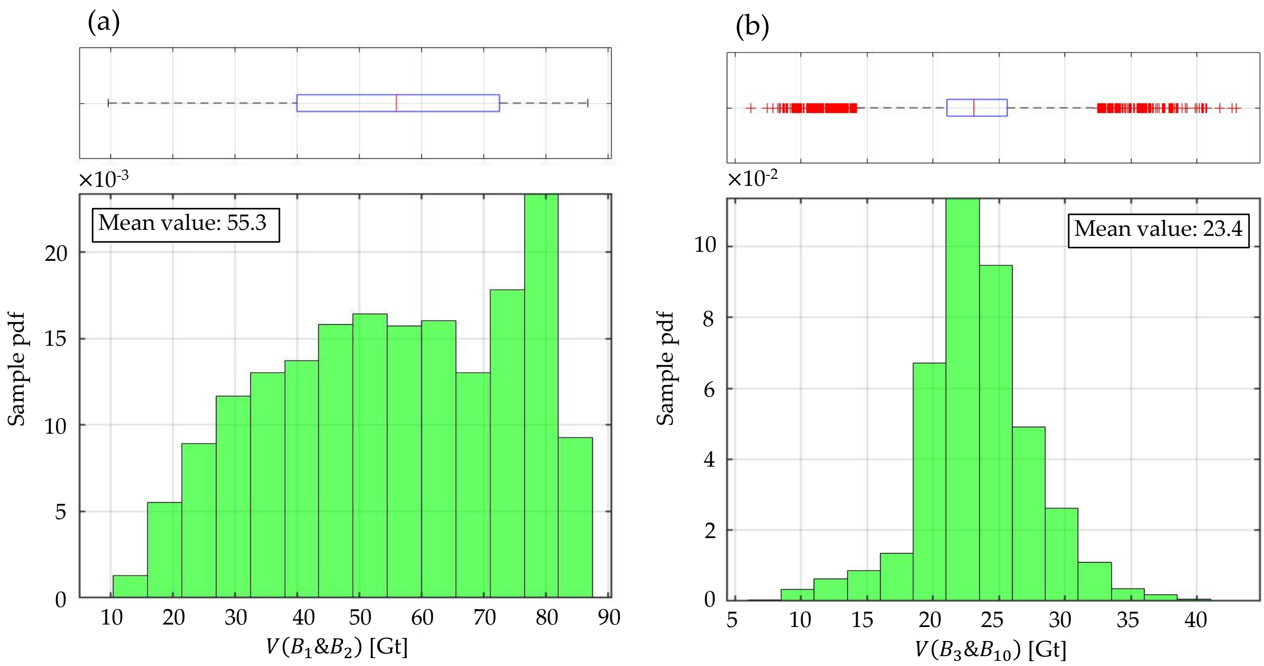

***Fig. 9**. Sample pdf of CO_2 storage capacity in the Erlin basin (with B_1 and B_2 subbasins) and Bohai Bay basin (with B_3 and B_{10} subbasins). Results correspond to 10^4 MC realizations for each basin/subbasin.*

Fig. 10 summarizes our results depicting the sample pdf of $V(B_{tot})$, corresponding to the overall storage capacity. For ease of interpretation, the associated boxplot representation is juxtaposed. This shows a median value of approximately 1350 Gt of CO_2 (red line) and an interquartile (25% to 75%) range spanning between 1100 and 1700 Gt of CO_2. As stated in Section 2.2, CO_2 emissions to be abated across China for the next 30 years are expected to range from 80 Gt of CO_2 (according to APS; IEA, 2021) to 175 Gt (without further intervention). These values are much lower than those associated with the probability distribution of $V(B_{tot})$ evaluated from our modeling approach (see Fig. 10). Accordingly, our probabilistic analysis supports the idea that the storage capacity of China can meet the needs of most of the CO_2 emissions and offers multiple possibilities to pair emission sources to storage sites.

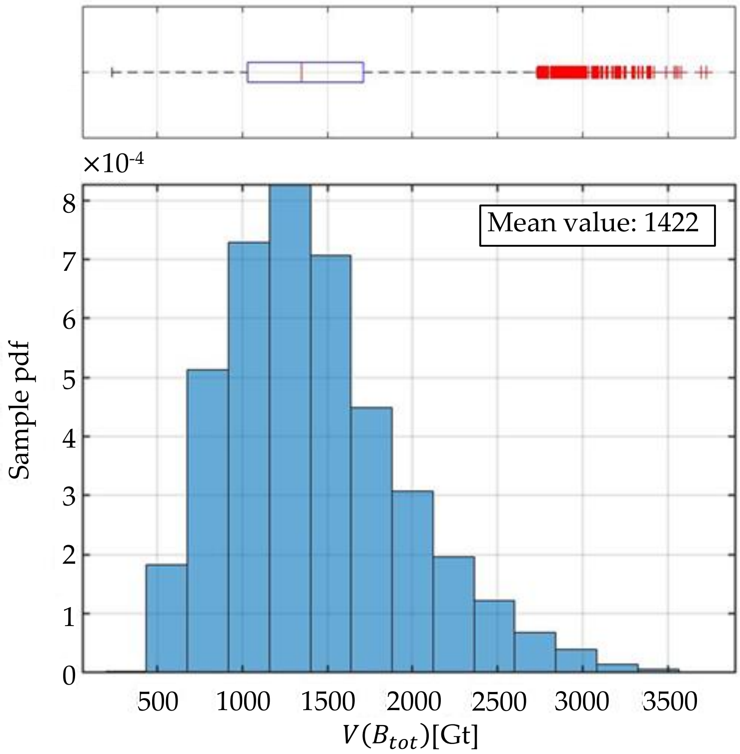

Fig. 10. *Sample pdf of total CO_2 storage capacity, $V(B_{tot})$, in the 10 studied basins across China. Results are based on 10^4 MC realizations for each basin.*

For example, if only the basins within the immediate proximity of the regions in China associated with the most severe carbon emissions are considered (i.e., the group denoted as B_s in Fig. 1b and comprising basins B_1 - B_5 and B_{10}), one can evaluate the total storage capacity available and assess the possibility that these basins fulfill the APS projected requirements of 80 Gt of CO_2. Fig. 11 depicts the sample pdf of storage capacity for group B_s. These results reveal an average storage capacity of about 93 Gt of CO_2 over the next 30 years, with lower and upper quartiles of 70 and 117 Gt of CO_2, respectively. Thus, our results suggest that group B_s is associated with about 68% probability of providing a storage capacity of at least 80 Gt of CO_2. Thus, this group of sites is potentially capable of satisfying the needs for CO_2 storage foreseen by APS within the year 2060.

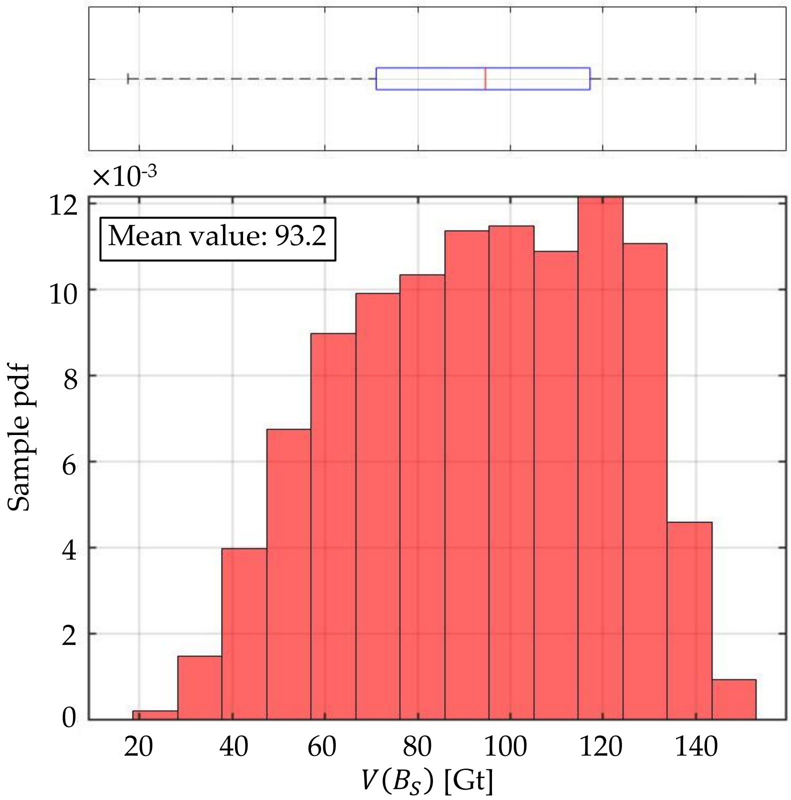

Fig. 11. *Sample pdf of total CO_2 storage capacity, $V(B_S)$, for 6 strategically selected basins of China. Results are based on 10^4 MC realizations for each storage basin.*

5. Conclusions

Carbon capture and storage is a key technology needed to reach net-zero. This study provides an estimate of the total storage capacity in major sedimentary basins in China close to emissions sources. A total of 10 basins are analyzed to estimate onshore CO_2 storage capacity in China. Capacity is constrained using a semi-analytical model of pressure build-up.

Uncertainties in the estimation of each basin storage capacity are evaluated in a numerical Monte Carlo simulation framework based on a collection of basin model realizations generated with different plausible input geological properties.

This study suggests that an average of 1350 Gt of CO_2 (with lower and upper quartiles of 1100 and 1700 Gt of CO_2, respectively) can be stored in onshore geological formations in eastern China within the next 30 years. In this context, considering the current emission scenario yields the expectation that up to 175 Gt of CO_2 will be emitted across China over the next 30 years. Meanwhile, according to the Announced Pledges Scenario suggested by IEA (IEA, 2021) China will require about 80 Gt carbon capture and storage over the next 30 years. Hence, our analysis supports the conclusion that that CCS technology can fully sustain the currently foreseen needs of CO_2 storage in China.

The results of the study suggest that a group of six basins can provide a viable answer to the needs for geological CO_2 storage in China by 2060. This subgroup is close to major emissions sources and may have sufficient capacity alone to store likely emissions for the next 30 years.

Application of a rigorous Global Sensitivity Analysis framework provides insights into (*i*) the most important (uncertain) model parameters affecting CO_2 storage capacity, and (*ii*) how these quantities affect the ensuing probability distribution of storage capacity. The GSA results show that for the basins with very low permeability rocks it is misleading to evaluate storage capacity referring to the size of reservoir. Instead, formation properties are the key parameters effecting pressure build-up and storage capacity of such reservoirs.

The results provided in this work can be used as a first step for further decision making, detailed investigations, and development of CCS projects. The uncertainty analysis performed offers critical insights on the most important parameters in storage assessment, providing suggestions for further data acquisition. Important sources of uncertainties that deserve future research include an assessment of the impact of reservoir heterogeneity and better characterization of formation properties. Coping with the combined effects of such sources of uncertainty would require significant theoretical and operational work to incorporate model and parameter uncertainties in the analysis and is still an open research challenge. Further source-sink matching analysis can also contribute to assist an economical and feasible implementation of CCS technology in China.

Conflicts of interest/Competing interests

The authors declare they have no known of conflicts of interest or competing interest that could have appeared to influence the work reported in this paper.

Availability of data and material

Data are available upon request

Authors' contributions

Ranaee, E. Software, design and implementation of the research, methodology, analysis of the results, writing - original draft, review. **Khattar, R.** Software, implementation of the research, investigation, methodology, data curation, analysis of the results, writing - original draft. **Inzoli, F.** design and supervision of the research, conceptualization, methodology, analysis of the results, writing, review & editing. **Blunt, M.J.** design and supervision of the research, conceptualization, methodology, analysis of the results, writing, review & editing**. Guadagnini, A.** design and supervision of the research, conceptualization, methodology, analysis of the results, writing, review & editing.

Consent for publication

All authors have read and agreed to the published version of the manuscript.

References

Ajayi, T.; Gomes, J. S.; Bera, A., 2019. A review of CO_2 storage in geological formations emphasizing modeling, monitoring and capacity estimation approaches. Petroleum Science, 16, 1028-1063. https://doi.org/10.1007/s12182-019-0340-8.

Bachu, S., 2008. CO_2 storage in geological media: Role, means, status and barriers to deployment. Prog. Energy Combust. Sci., 34, 254-273. https://doi.org/10.1016/J.PECS.2007.10.001

Bachu, S., Bonijoly, D., Bradshaw, J., Burruss, R., Holloway, S., Christensen, N.P., Mathiassen, O.M., 2007. CO_2 storage capacity estimation: Methodology and gaps. Int. J. Greenh. Gas Control., 1(4), 430-443. https://doi.org/10.1016/S1750-5836(07)00086-2

Bachu, S., 2003. Screening and ranking of sedimentary basins for sequestration of CO_2 in geological media in response to climate change. Environmental Geology, 44, 277-289. https://doi.org/10.1007/s00254-003-0762-9

Barros, E. G. D., Leeuwenburgh, O., Szklarz, S., 2021. Quantitative assessment of monitoring strategies for conformance verification of CO_2 storage projects, Int. J. Greenh. Gas Control., 110 (2021) 103403. https://doi.org/10.1016/j.ijggc.2021.103403

Bianchi Janetti, E., Guadagnini, L., Riva, M., Guadagnini, A., 2019. Global sensitivity analyses of multiple conceptual models with uncertain parameters driving groundwater flow in a regional-scale sedimentary aquifer. Journal of Hydrology, 574, 544-556. https://doi.org/10.1016/j.jhydrol.2019.04.035

Bruce Hill, L., Li, X.C., Wei, N., 2020. CO_2-EOR in China: A comparative review, Int. J. Greenh. Gas Control. 103, 103173. https://doi.org/10.1016/j.ijggc.2020.103173

Celia, M. A., 2017. Geological storage of captured carbon dioxide as a large-scale carbon mitigation option. In Water Resources Research, 53(5), 3527-3533. https://doi.org/10.1002/2017WR020841

China Energy Council (CEC), 2021. Analysis and Forecast of China Power Demand-Supply Situation 2020-2021, https://english.cec.org.cn/detail/index.html?3-1128

Chu, J., Zhang, C., Fu, G., Li, Y., Zhou, H., 2015. Improving multi-objective reservoir operation optimization with sensitivity-informed dimension reduction. Hydrology and Earth System Sciences, 19, 3557-3570. https://doi.org/10.5194/hess-19-3557-2015

Cooney, G., Littlefield, J., Marriott, J., Skone, T. 2015. Evaluating the climate benefits of CO_2-Enhanced oil recovery using life cycle analysis. Environ. Sci. Technol. 49. https://doi.org/10.1021/acs.est.5b00700

Cooper, H. H.; Jacob, C. E., 1946. A generalized graphical method for evaluating formation constants and summarizing well- field history. Eos, Transactions American Geophysical Union, 27(4), 526-534. https://doi.org/10.1029/TR027i004p00526

Corless, R., Gonnet, G., Hare, D., Jeffrey, D., Knuth, D., 1996. On the Lambert W Function. Advances in Computational Mathematics, 5, 329-359. https://doi.org/10.1007/BF02124750

Cui, D., Liu, Z., Duan, C., Deng, Z., Deng, X., Song, X., Dou, X., Sun, T., 2021. Daily CO_2 emission for China's provinces in 2019 and 2020. Earth System Science Data Discussions. https://doi.org/10.5194/essd-2021-153

Dahowski, R. T., Li, X., Dooley, J. J., 2009. Regional Opportunities for Carbon Dioxide Capture and Storage in China The effective pressure law for permeability of clay-rich sandstones View project Demonstration of Key Technologies for Clean and Efficient Utilization of Low-Rank Coal, R&D of CO_2 Geological Storage View project. https://doi.org/10.2172/990594

De Simone, S., Krevor, S., 2021. A tool for first order estimates and optimization of dynamic storage resource capacity in saline aquifers. Int. J. Greenh. Gas Control., 106, 103258. https://doi.org/10.1016/j.ijggc.2021.103258

Degenring, D., Röhl, M., Uhrmacher, A. M., 2004. Discrete event, multi-level simulation of metabolite channeling. BioSystems, 75(1–3), 29-41. https://doi.org/10.1016/j.biosystems.2004.03.008

Dell'Oca, A., Riva, M., Guadagnini, A., 2017. Moment-based metrics for global sensitivity analysis of hydrological systems. Hydrology and Earth System Sciences, 21(12), 6219–6234. https://doi.org/10.5194/hess-21-6219-2017

Diao, Y., Zhu, G., Cao, H., Zhang, C., Li, X., Jin, X., 2017. Mesoscale assessment of CO2 storage potential and geological suitability for target area selection in the Sichuan Basin. Geofluids, 2017, 9587872. https://doi.org/10.1155/2017/9587872

Fan, J., Guo, J., Zhang, S., Ji, X., 2014. CO_2 Geological Storage Suitability Assessment of Sichuan Basin. Journal of Applied Mathematics and Physics, 2, 1009-1021. https://doi.org/10.4236/jamp.2014.211115

Food and Agriculture Organisation of the United Nations (FAO) 2021. FAOSTAT Data, http://www.fao.org/faostat/en/#data, accessed August 2021.

Friedlingstein, P., O'Sullivan, M., Jones, M. W., Andrew, R. M., Hauck, J., Olsen, A., Peters, G. P., Peters, W., Pongratz, J., Sitch, S., le Quéré, C., Canadell, J. G., Ciais, P., Jackson, R. B., Alin, S., Aragão, L. E. O. C., Arneth, A., Arora, V., Bates, N. R., … Zaehle, S., 2020. Global Carbon Budget 2020. Earth System Science Data, 12(4), 3269-3340. https://doi.org/10.5194/essd-12-3269-2020

Godec, M.L., 2011. Global Technology Roadmap for CCS in Industry. Sectoral Assessment CO2 Enhanced Oil Recovery. Advanced Resources International, Arlington VA USA. https://www.unido.org/sites/default/files/2011-05/EOR_0.pdf

He, J., Li, Z., Zhang, X., Wang, H., Dong, W., Chang, S., Ou, X., Guo, S., Tian, Z., Gu, A., Teng, F., Yang, X., Chen, S., Yao, M., Yuan, Z., Zhou, L., Zhao, X., 2020. Comprehensive report on China's Long-Term Low-Carbon Development Strategies and Pathways. Chinese Journal of Population, Resources and Environment, 18(4), 263-295. https://doi.org/10.1016/j.cjpre.2021.04.004

Hill, P. L., Turiano, N. A., Mroczek, D. K., Burrow, A. L., 2016. The value of a purposeful life: Sense of purpose predicts greater income and net worth. Journal of Research in Personality, 65, 38-42. https://doi.org/10.1016/j.jrp.2016.07.003

IEA (International Energy Agency). 2021. An Energy Sector Roadmap to Carbon Neutrality in China. CC BY-NC 3.0 IGO.

IEA (International Energy Agency). 2020. Energy Technology Perspectives 2020, IEA, Paris https://www.iea.org/reports/energy-technology-perspectives-2020.

IPCC, 2018. Summary for Policymakers. In: *Global Warming of 1.5°C. An IPCC Special Report on the impacts of global warming of 1.5°C above pre-industrial levels and related global greenhouse gas emission pathways, in the context of strengthening the global response to the threat of climate change, sustainable development, and efforts to eradicate poverty*. *World Meteorological Organization, Geneva, Switzerland, 32 pp.*

Jaeger, J. C., Cook, N. G. W., Zimmerman, R., 2009. Fundamentals of Rock Mechanics, 4th Edition, John Wiley and Sons.

Jiao, Z., Surdam, R. C., Zhou, L., Stauffer, P. H., Luo, T., 2011. A feasibility study of geological CO2 sequestration in the Ordos Basin, China. Energy Procedia, 4, 5982-5989. https://doi.org/10.1016/j.egypro.2011.02.601

Jin, C., Liu, L., Li, Y., Zeng, R., 2017. Capacity assessment of CO2 storage in deep saline aquifers by mineral trapping and the implications for Songliao Basin, Northeast China. Energy Science and Engineering, 5(2), 81-89. https://doi.org/10.1002/ese3.151

Karvounis, P., Blunt, M. J., 2021. Assessment of CO2 geological storage capacity of saline aquifers under the North Sea. Int. J. Greenh. Gas Control., 111, 103463. https://doi.org/10.1016/j.ijggc.2021.103463

Kullback, S., Leibler, R. A., 1951. On Information and Sufficiency. The Annals of Mathematical Statistics, 22(1), 79-86. https://doi.org/10.1214/aoms/1177729694

Li, Q., Liu, G., 2016. Risk Assessment of the Geological Storage of CO2: a Review, Geologic Carbon Sequestration. Springer.

Li, X., Wei, N., Jiao, Z., Liu, S., Dahowski, R., 2019. Cost curve of large-scale deployment of CO2-enhanced water recovery technology in modern coal chemical industries in China. Int. J. Greenh. Gas Control. 81, 66-82. https://doi.org/10.1016/j.ijggc.2018.12.012

Li, X., Wei, N., Liu, Y., Fang, Z., Bai, B., Dahowski, R., Davidson, C., 2009. CO2 point emission and geological storage capacity in China. IOP Conference Series: Earth and Environmental Science, 6, 172026. https://doi.org/10.1088/1755-1307/6/7/172026

Leung, D. Y. C., Caramanna, G., Maroto-Valer, M. M., 2014. An overview of current status of carbon dioxide capture and storage technologies. Renewable and Sustainable Energy Reviews, 39, 426-443. https://doi.org/10.1016/j.rser.2014.07.093

Mechler, R., Singh, C., Ebi, K., Djalante, R., Thomas, A., James, R., Revi, A., 2020. Loss and Damage and limits to adaptation: recent IPCC insights and implications for climate science and policy. Sustainability Science, 15(4),1245-1251. https://doi.org/10.1007/s11625-020-00807-9

Michael, K., Neal, P.R., Allinson, G., Ennis-King, J., Hou, W., Paterson, L., Sharma, S., Aiken, T., 2011. Injection strategies for large-scale CO2 storage sites. Energy Procedia. 4, 4267-4274. doi:10.1016/j.egypro.2011.02.376

Muleta, M. K., Nicklow, J. W., 2005. Sensitivity and uncertainty analysis coupled with automatic calibration for a distributed watershed model. Journal of Hydrology, 306(1–4), 127-145. https://doi.org/10.1016/j.jhydrol.2004.09.005

National Bureau of Statistics of China 2008. http://www.stats.gov.cn/english/

Nordbotten, J. M., Celia, M. A., Bachu, S., 2005. Injection and storage of CO2 in deep saline aquifers: Analytical solution for CO2 plume evolution during injection. Transport in Porous Media, 58, 339-360. https://doi.org/10.1007/s11242-004-0670-9

Nossent, J., Elsen, P., Bauwens, W, 2011. Sobol' sensitivity analysis of a complex environmental model, Environmental Modelling and Software, 26(12), 1515-1525. https://doi.org/10.1016/j.envsoft.2011.08.010

Pappenberger, F., Beven, K. J., Ratto, M., Matgen, P., 2008. Multi-method global sensitivity analysis of flood inundation models. Advances in Water Resources, 31(1), 1–14. https://doi.org/10.1016/j.advwatres.2007.04.009

Petroleum Geology of China. 1992. Chinese Petroleum Geology Editorial Committee, CPGEC. Petroleum industry press.

Poulsen, N., Chen, W., Dai, S., Ding, G., Li, M., Vincent, C., Zeng, R., 2011. Geological assessment for CO2 storage in the Bahaiwan Basin, East China. Energy Procedia, 4, 5990–5998. https://doi.org/10.1016/j.egypro.2011.02.602

Punzo, V., Montanino, M., Ciuffo, B., 2015. Do we really need to calibrate all the parameters? Variance-based sensitivity analysis to simplify microscopic traffic flow models. IEEE Transactions on Intelligent Transportation Systems, 16(1), 184-193. https://doi.org/10.1109/TITS.2014.2331453

Qiao, X., Li, G., Li, M., Wang, Z., 2012. CO2 storage capacity assessment of deep saline aquifers in the Subei Basin, East China. Int. J. Greenh. Gas Control., 11, 52-63. https://doi.org/10.1016/j.ijggc.2012.07.020

Ranaee, E., Ghorbani, H., Keshavarzian, S., Ghazaeipour Abarghoei, P., Riva, M., Inzoli, F., Guadagnini, A., 2021a. Analysis of the performance of a crude-oil desalting system based on historical data. Fuel, 291, 120046. https://doi.org/10.1016/j.fuel.2020.120046

Ranaee, E., Abbasi, A.A., Tabatabaee, J., Ziyaee, M., 2021b. Feasibility of Rainwater Harvesting and Consumption in a Middle Eastern Semiarid Urban Area, Water, 13(15), 2130. https://doi.org/10.3390/w13152130

Ruano, M. V., Ribes, J., Seco, A., Ferrer, J., 2012. An improved sampling strategy based on trajectory design for application of the Morris method to systems with many input factors. Environmental Modelling and Software, 37, 103-109. https://doi.org/10.1016/j.envsoft.2012.03.008

Russian, A., Riva, M., Russo, E. R., Chiaramonte, M. A., Guadagnini, A., 2019. Stochastic inverse modeling and global sensitivity analysis to assist interpretation of drilling mud losses in fractured formations. Stochastic Environmental Research and Risk Assessment, 33, 1681-1697. https://doi.org/10.1007/s00477-019-01729-4

Rutqvist, J., 2012. The Geomechanics of CO2 Storage in Deep Sedimentary Formations. Geotechnical and Geological Engineering, 30, 525-551. https://doi.org/10.1007/s10706-011-9491-0

Saltelli, A., Ratto, M., Andres, T., Campolongo, F., Cariboni, J., Gatelli, D., Saisana, M., Tarantola, S., 2008. Global sensitivity analysis: The primer. Global Sensitivity Analysis: The Primer, John Wiley and Sons. https://doi.org/10.1002/9780470725184

Saunois, M., Stavert, A. R., Poulter, B., Bousquet, P., Canadell, J. G., Jackson, R. B., ... Zhuang, Q., 2020. The global methane budget 2000-2017. Earth System Science Data, 12(3), 1561-1623. https://doi.org/10.5194/essd-12-1561-2020

Sifuentes, W. F., Giddins, M. A., Blunt, M. J., 2009. Modeling CO2 Storage in Aquifers: Assessing the Key Contributors to Uncertainty. SPE-123582-MS. Offshore Europe, Aberdeen, UK. https://doi.org/10.2118/123582-MS

Sobol', I. M., 1993. Sensitivity Estimates for Nonlinear Mathematical Models. Mathematical Modeling and Computational experiment, 1(4), 407-414.

Su, X., Xu, W., Du, S., 2013. Basin-scale CO2 storage capacity assessment of deep saline aquifers in the Songliao Basin, northeast China. Greenhouse Gases: Science and Technology 3(4), 266-280. https://doi.org/10.1002/ghg.1354

Sudret, B., 2008. Global sensitivity analysis using polynomial chaos expansions. Reliability Engineering and System Safety, 93(7), 964-979. https://doi.org/10.1016/j.ress.2007.04.002

Sun, X., Alcalde, J., Gomez-Rivas, E., Struth, L., Johnson, G., Trave, A. 2021. Appraisal of CO2 storage potential in compressional hydrocarbon-bearing basins: Global assessment and case study in the Sichuan Basin (China). Geoscience Frontiers. 11, 2309-2321. https://doi.org/10.1016/j.gsf.2020.02.008

Szulczewski, M. L., MacMinn, C. W., Herzog, H. J., Juanes, R., 2012. Lifetime of carbon capture and storage as a climate-change mitigation technology. Proceedings of the National Academy of Sciences of the United States of America, 109(14) 5185-5189. https://doi.org/10.1073/pnas.1115347109

United Nations Framework Convention on Climate Change (UNFCCC). 2021. *Greenhouse Gas Data, https://unfccc.int/process-and-meetings/transparency-andreporting/greenhouse-gas-data/ghg-data-unfccc/ghg-data-from-unfccc, accessed August 2021.*

van Griensven, A., Meixner, T., Grunwald, S., Bishop, T., Diluzio, M., Srinivasan, R., 2006. A global sensitivity analysis tool for the parameters of multi-variable catchment models. Journal of Hydrology, 324(1-4), 10-23. https://doi.org/10.1016/j.jhydrol.2005.09.008

Villarasa, V., Bolster, D., Dentz, M., Olivella, S., Carrera, J., 2010. Effects of CO2 compressibility on CO2 storage in deep saline aquifers. Transp. In Porous Media, 85, 619-639. https://doi.org/10.1007/s11242-010-9582-z.

Vincent, C., Dai, S., Wenying, C., Zeng, R., Guosheng, D., Xu, R., Dalhoff, F., 2009. Carbon dioxide storage options for the COACH project in the Bohai Basin, China. Energy Procedia, 1, 2785-2792. https://doi.org/10.1016/j.egypro.2009.02.050

Wagener, T., van Werkhoven, K., Reed, P., Tang, Y., 2009. Multiobjective sensitivity analysis to understand the information content in streamflow observations for distributed watershed modeling. Water Resources Research, 45(2), W02501. https://doi.org/10.1029/2008WR007347

Wang, S., Vincent, C. J., Stephenson, M. H., Zeng, R., 2014. Assessment of storage capacity for CO2 in saline aquifers near hydrocarbon fields, northern Songliao Basin, China. Greenhouse Gases: Science and Technology, 4(3), 366-383. https://doi.org/https://doi.org/10.1002/ghg.1398

Wang, S., Vincent, C. J., Zeng, R., Stephenson, M. H., 2018. Geological suitability and capacity of CO2 storage in the Jiyang Depression, East China. Greenhouse Gases: Science and Technology, 8(4), 747-761. https://doi.org/10.1002/ghg.1782

Wei, N., Li, X., Wang, Y., Dahowski, R. T., Davidson, C. L., Bromhal, G. S., 2013. A preliminary sub-basin scale evaluation framework of site suitability for onshore aquifer-based CO2 storage in China. Int. J. Greenh. Gas Control., 12, 231-246. https://doi.org/10.1016/j.ijggc.2012.10.012

Wei, N., Li, X., Dahowski, R.T., Davidson, C.L., Liu, S., Zha, Y., 2015. Economic evaluation on CO2 -EOR of onshore oil fields in China. Int. J. Greenh. Gas Control. 37, 170-181. https://doi.org/10.1016/j.ijggc.2015.01.014

Zhang, L., Ren, B., Huang, H., Li, Y., Ren, S., Chen, G., Zhang, H., 2015. CO2 EOR and storage in Jilin Oilfield: monitoring program and preliminary results. J. Pet. Sci. Eng. 125, 1-12. https://doi.org/10.1016/j.petrol.2014.11.005

Zeng, R., Vincent, C. J., Tian, X., Stephenson, M. H., Wang, S., Xu, W., 2013. New potential carbon emission reduction enterprises in China: Deep geological storage of CO2 emitted through industrial usage of coal in China. Greenhouse Gases: Science and Technology, 3(2), 106-115. https://doi.org/10.1002/ghg.1314

Zhou, D., Zhao, Z., Liao, J., Sun, Z., 2011. A preliminary assessment on CO2 storage capacity in the Pearl River Mouth Basin offshore Guangdong, China. Int. J. Greenh. Gas Control., 5(2), 308-317. https://doi.org/10.1016/j.ijggc.2010.09.011